Ageing disrupts MANF-mediated immune modulation during skeletal muscle regeneration

Neuza S. Sousa[1], Margarida F. Brás[1], Inês B. Antunes[1], Päivi Lindholm[2], Joana Neves[1*], Pedro Sousa-Victor[1*]

[1]Instituto de Medicina Molecular João Lobo Antunes, Faculdade de Medicina, Universidade de Lisboa, Portugal

[2]Institute of Biotechnology, Helsinki Institute of Life Science HiLIFE, University of Helsinki, 00014, Helsinki, Finland

*Correspondence to:

J. Neves and P. Sousa-Victor

Address:

Instituto de Medicina Molecular, Faculdade de Medicina de Lisboa, Av. Prof. Egas Moniz, Edifício Egas Moniz, 1649-028 Lisboa, Portugal.

E-mail: joana.neves@medicina.ulisboa.pt; psvictor@medicina.ulisboa.pt

Phone: (+351) 217 999 411

Abstract

Age-related decline in skeletal muscle regenerative capacity is multifactorial, yet, the contribution of immune dysfunction to regenerative failure is unknown. Macrophages are essential for effective debris clearance and MuSC activity during muscle regeneration, but the regulatory mechanisms governing macrophage function during muscle repair are largely unexplored. Here, we uncover a new mechanism of immune modulation operating during skeletal muscle regeneration that is disrupted in aged animals and relies on the regulation of macrophage function. The immune modulator MANF is induced following muscle injury in young mice, but not in aged animals, and its expression is essential for regenerative success. Regenerative impairments in the aged muscle are associated with defects in the repair-associated myeloid response similar to those found in MANF-deficient models and could be improved through MANF delivery. We propose that restoring MANF levels is a viable strategy to improve myeloid response and regenerative capacity in the aged muscle.

Main text

Age-related decline in regenerative capacity is the synergistic result of cell intrinsic impairments in somatic stem cells and alterations in the local and systemic environment coordinating the repair process[1,2]. The reversible nature of some of the age-associated changes affecting the regenerative environment has been demonstrated through heterochronic parabiosis experiments, where old tissue is exposed to a youthful circulatory environment, highlighting the potential of interventions in the aged tissue milieu to reverse regenerative decline[3,4]. The myeloid system is a potential candidate to mediate these rejuvenating effects[5-7].

The skeletal muscle is a paradigmatic model to study age-related loss of regenerative capacity. Skeletal muscle regeneration is sustained throughout life by a population of adult muscle stem cells (MuSCs) and relies on a highly coordinated sequence of events, engaging several niche populations[8-10]. Immune cells infiltrate the skeletal muscle soon after injury and are responsible for essential functions, including the clearance of tissue debris and the coordinated regulation of MuSC function and other niche components[11,12]. Macrophages are the most abundant type of immune cells participating in muscle repair and originate from infiltrating monocytes that differentiate in situ into pro-inflammatory macrophages[12]. Regenerative success depends on a timely regulated phenotypic transition of these pro-inflammatory macrophages into pro-repair macrophages[12-14]. During this process CCR2^{pos}Ly6C^{High} macrophages mature into a different type of macrophages that lose Ly6C expression and acquire a new surface receptor, CX3CR1.

Recently, we identified a novel immune modulatory function for Mesencephalic Astrocyte-derived Neurotrophic Factor (MANF)[15], an endoplasmic reticulum (ER)-stress-inducible protein with pleiotropic effects in multiple organs[16-19]. We found that MANF is a systemic regulator of inflammation and tissue homeostasis during ageing, and one of the factors required in young blood to promote part of the rejuvenation effects elicited by heterochronic parabiosis[20]. Circulatory MANF levels decline with age in mice and humans, and MANF supplementation in old mice is sufficient to limit inflammation and tissue damage in the liver[20] and preserve retinal homeostasis[21].

However, how a decline in MANF signalling affects the age-related loss of regenerative capacity remains unexplored.

MANF is essential for muscle regeneration

To explore the involvement of MANF in muscle regeneration, we evaluated MANF expression following muscle injury. We observed a sharp increase in MANF levels that peaked at 3-4 days post injury (dpi) and progressively declined thereafter (Fig. 1a-b and Extended data 1a). Importantly, this injury-dependent induction of MANF was blunted in aged animals (Fig. 1c and Extended data 1b), revealing an inability of aged muscles to significantly induce MANF between 2 and 3dpi (Extended data 1c).

To understand the consequences of defective MANF signalling for muscle regeneration, we generated a mouse model allowing the inducible and ubiquitous ablation of MANF in adult animals. In the Rosa26-Cre[ER], Manf^{fl/fl} mice, tamoxifen treatment immediately before muscle injury and during muscle regeneration (Fig. 1d) resulted in a complete loss of MANF protein in the regenerating tissue (Extended data 1d). Analysis of tamoxifen-treated Rosa26-Cre[ER], Manf^{fl/fl} mice (herein referred to as Manf[R26Δ]), revealed impairments in muscle regeneration compared to oil treated mice (Manf[R26WT]) and tamoxifen-treated Manf^{fl/fl} mice. This is evidenced by a reduction in the density and the cross-sectional area (CSA) of new myofibres formed at 4dpi (Fig. 1e-h) and a persistence of necrotic myofibres within the regenerating muscle (Fig. 1e,i), resembling the phenotype found in aged animals[22,23].

Manf[R26Δ] mice also displayed a significant reduction in the number of MuSCs (p<0.01, Fig. 2a) and CD45^{pos} immune cells (p<0.05, Fig. 2b) in the regenerating muscle at 3dpi, with no changes in the populations of fibroadipogenic progenitors (FAPs) or endothelial cells (Extended data 2a-c). Considering the fundamental role of myeloid cells in the clearance of necrotic debris, a process impaired in Manf[R26Δ] mice, we focused our analysis on the repair-associated myeloid response. Manf[R26Δ] mice had a 65% reduction in the number of myeloid cells (CD11b^{pos}) at 3dpi, corresponding to an 82% reduction in the pro-repair (F4/80^{pos}Ly6C[Low]) macrophage population and a less pronounced reduction in the pro-inflammatory (Ly6C[High]) population (p=0.06, Fig. 2c-e and Extended data 2d). The neutrophil population was unchanged (Extended data 2e). Thus, MANF loss is associated with defects in the repair-associated myeloid response characterized by a reduced presence of myeloid cells in the injured muscle and an imbalance in macrophage states, whereby pro-inflammatory macrophages tend to accumulate at the expense of pro-repair macrophages.

Ageing impairs the repair-associated myeloid response

Skeletal muscle from aged animals exhibits regenerative defects similar to those found in Manf[R26Δ] mice[22,23] and a blunted induction of MANF following injury (Fig. 1c and Extended data 1b-c). Thus, we asked whether this reduction in MANF levels in aged muscles was associated with similar defects in the repair-associated myeloid response. We found that 23-25mo old animals had a 41% reduction in the number of myeloid cells within the regenerating skeletal muscle at 3dpi (Fig. 2f and Extended data 2f), with a 55% reduction in the number of pro-repair macrophages and no

significant changes in the number of pro-inflammatory macrophages (Fig. 2g-i). Importantly, these defects manifested as a reduced capacity to increase the total number of myeloid cells and pro-repair macrophages between 2 and 3 dpi (Extended data 2g-i). Thus, aged muscles display defects in myeloid cell accumulation and an imbalance of macrophage subpopulations that can be recapitulated in conditions of MANF loss. This parallel in myeloid defects included only the macrophage populations and not the neutrophil population, which was reduced in aged animals but not in Manf[R26Δ] mice (Extended data 2e-f).

MANF is induced in pro-repair macrophages after injury

Since MANF is induced in macrophages after injury in other systems[15] and macrophage numbers increase in the skeletal muscle following injury (Extended data 3a, see also REF[12]), we hypothesized that macrophages could be a source of MANF in the regenerating skeletal muscle. Indeed, F4/80^{pos} cells immunostained in muscle cryosections co-localized with sites of highest MANF expression (Extended data 3b). To further test this hypothesis we treated mice with clodronate liposomes during muscle injury, generating a condition where macrophage numbers are reduced, but neutrophils are not affected (Fig. 3a and Extended data 3c, see also REFS[24-26]), and observed a significant reduction in the levels of MANF protein present in the skeletal muscle at 3dpi ($p < 0.05$, Fig. 3b). To distinguish whether the increase in MANF levels is due to the influx of macrophages following muscle injury or the induction of MANF within the macrophage population, we isolated F4/80^{pos} cells by fluorescence activated cell sorting (FACS) and analyzed MANF protein expression. Interestingly, MANF protein levels were also changed in the F4/80[pos] population of macrophages (Fig. 3c), mimicking the expression dynamic observed in whole muscles (Fig. 1a-b) and following the phenotypic transition of pro-inflammatory macrophages into pro-repair macrophages during muscle repair (Extended data 3d, see also REF[27]). Consistently, analysis of isolated macrophage subpopulations revealed that MANF is specifically induced in the F4/80[pos]Ly6C[Low] subpopulation of pro-repair macrophages (Fig. 3d).

To confirm that this population is the main source of MANF during muscle regeneration we generated a mouse model to selectively deplete MANF in the emerging population of pro-repair macrophages that specifically express Cx3cr1[27]. Indeed, tamoxifen-treated Cx3cr1-Cre[ER], Manf^{fl/fl} mice (herein referred to as Manf[Cx3cr1Δ]), displayed a complete ablation of MANF protein within the F4/80[pos] population of macrophages (Fig. 3e) and an 80% reduction in MANF levels in whole muscles (Fig. 3f) when compared to oil treated mice (Manf[Cx3cr1WT]). These data support the idea that MANF induction following muscle injury is not only due to an influx of macrophages to the site of injury, but mostly, to a specific increase in MANF protein levels associated with the emergence of pro-repair macrophages within the injured muscle.

MANF ablation in Cx3cr1^{pos} cells impairs regeneration

To understand the consequences of MANF loss in Cx3cr1^{pos} cells we analyzed Manf[Cx3cr1Δ] animals on a time course following muscle injury, evaluating the repair-associated myeloid response and the efficiency of regeneration (Fig. 4a). Analysis of myeloid cell populations in Manf[Cx3cr1Δ] mice revealed alterations in the dynamics of the transition between macrophage phenotypes and a

4

reduced presence of myeloid cells within the skeletal muscle (Fig. 4b-f). These alterations were characterized by a significant reduction in the number of pro-repair macrophages ($p < 0.0001$ at 3dpi, Fig. 4d), and no alterations in the numbers of pro-inflammatory macrophages (Fig. 4e), causing a reduction in the ratio of pro-repair to pro-inflammatory macrophages at 3 dpi (Fig. 4f). Importantly, changes in myeloid populations were not due to the tamoxifen treatment, as they were still observed when Manf$^{Cx3cr1\Delta}$ mice were compared with tamoxifen-treated Manf$^{fl/fl}$ mice as controls (Extended data 4a-c).

Evaluation of regenerating muscles revealed that MANF ablation in Cx3cr1^{pos} cells was sufficient to cause defects in muscle repair, evidenced by a reduction in the number of MuSCs present at 3dpi (Fig. 4g), reduced CSA of new myofibres and increased presence of necrotic fibres at 4dpi, that persisted at 14dpi (Fig. 4h-k and Extended data 4d-f), despite no defects being detected prior to injury (Extended data 4g). Thus, MANF derived from Cx3cr1^{pos} cells is essential for a regulated myeloid response, successful debris clearance following muscle injury, and effective muscle regeneration.

MANF is a regulator of the phenotypic transition of macrophages

Interestingly, the defects in the repair-associated myeloid response observed in Manf$^{Cx3cr1\Delta}$ animals were not detected at 1dpi and developed primarily between 2dpi and 3dpi (Fig. 4c-f), suggesting that they are associated with specific mechanisms operating during the process of transition of macrophage phenotypes. Indeed, tamoxifen treatment of Cx3cr1-Cre^{ER}, Manf$^{fl/fl}$ mice only prior to the injury (and not during the injury) did not result in any defects in the repair-associated myeloid response (Extended data 5a-d), supporting the idea that the defects observed are due to MANF-ablation in Cx3cr1^{pos} cells that appear only during the injury and not Cx3cr1^{pos} resident macrophages or Cx3cr1^{pos} non-classical monocytes. Consistently, we did not observe any alterations in myeloid cell composition in the skeletal muscle of Manf$^{Cx3cr1\Delta}$ animals in homeostasis (Extended data 5e-f), nor in the blood of Manf$^{Cx3cr1\Delta}$ animals in homeostasis or after injury (Extended data 5g-i). Moreover, proliferation (evaluated by EdU incorporation between 2 and 3dpi), and apoptosis (evaluated by Apopxin Green indicator) was not different in the macrophage populations present in the skeletal muscle at 3 dpi (Extended data 5j-m). This analysis supports the idea that the myeloid defects observed in Manf$^{Cx3cr1\Delta}$ animals are likely associated with impairment in the process of phenotypic transition in the macrophage population.

To explore the potential role of MANF in macrophage's phenotypic transition *ex vivo*, we generated an additional mouse model where MANF is ablated in macrophages in a tamoxifen-independent manner (Manf$^{LysM\Delta}$ mice). Similarly to Manf$^{Cx3cr1\Delta}$ mice, Manf$^{LysM\Delta}$ mice had lower numbers of myeloid cells within the regenerating muscle and a delayed transition between macrophage phenotypes when compared to Manf$^{fl/fl}$ mice (Extended data 6a-e).

To evaluate a specific role of MANF in macrophages' phenotypic transition, we developed an *ex vivo* assay that allows us to follow the transition of pro-inflammatory macrophages into pro-repair macrophages, independently of the alterations in myeloid cell numbers. In this assay, single cell suspensions isolated from 2dpi muscles were cultured for 16h and the distribution of macrophage populations was quantified by flow cytometry at 0h and 16h. Cultured macrophages recapitulated

the phenotypic transition observed *in vivo* (Fig. 5a), which can be quantified by the loss of Ly6C marker (Fig. 5a-b). Indeed, Manf$^{LysM\Delta}$ mice showed defects in the process of phenotypic transition ex-vivo, evidenced by a higher percentage of cells retaining the Ly6C^{High} status after 16h in culture (Fig. 5c). Importantly, these defects could be ameliorated by supplementing recombinant MANF (rMANF) protein in the culture media (Fig. 5c), suggesting a feed-forward autocrine mechanism by which MANF derived from pro-repair macrophages sustains the formation of new pro-repair macrophages. Since the percentage of Ly6C^{High} macrophages is already higher at 0h in Manf$^{LysM\Delta}$ mice it is possible that the differences we observed at 16h were also a reflection of this initial delay. Thus, we repeated this experiment using Ly6C^{High} macrophages isolated by FACS. Indeed, Ly6C^{High} macrophages from Manf$^{LysM\Delta}$ mice showed significant impairments in performing the phenotypic transition when compared to Manf$^{fl/fl}$ mice, evaluated by the ability to downregulate Ly6C expression (Fig. 5d-e). This observation was further confirmed in Ly6C^{High} macrophages isolated by FACS from Manf$^{R26\Delta}$ mice: RNA analysis of macrophages followed for 20h in culture after sorting showed that macrophages isolated from tamoxifen-treated Manf$^{fl/fl}$ mice up-regulate Manf and Cx3cr1, indicative of an efficient process of phenotypic transition that parallels what is observed *in vivo*. On the contrary, macrophages isolated from Manf$^{R26\Delta}$ mice had negligible levels of Manf expression and showed significant defects in the induction of Cx3cr1 (Fig. 5f). Finally, intrinsic defects in MANF-deficient macrophages were also confirmed in bone marrow-derived macrophage (BMDM) cultures generated from Manf^{R26WT} and Manf$^{R26\Delta}$ mice. Manf^{KO} macrophages had higher levels of pro-inflammatory genes and induced a stronger pro-inflammatory response after stimulation with Fibrinogen, a common signal present during muscle regeneration (Extended data 6f). Collectively, this analysis support the idea that that MANF is an essential autocrine regulator of macrophages' phenotypic transition during muscle regeneration and is important to limit excessive pro-inflammatory signaling.

MANF-deficient macrophages have reduced lysosomal activity

RNA sequencing (RNAseq) analysis of macrophages (CD45^{pos}F4/80^{pos}) freshly isolated from Manf$^{Cx3cr1\Delta}$ and Manf^{Cx3cr1WT} muscles at 3dpi revealed changes in key cellular processes (Fig. 6a-b and Extended data 7a). Gene ontology analysis of the dataset of down-regulated genes revealed enrichment for genes associated with lysosomal and endosomal compartments (Fig. 6a), and with molecular functions related to hydrolase, peroxidase and oxidoreductase activity (Fig. 6b). Consistently, functional classification of all differentially expressed genes revealed alterations in the biological processes of MHC class II antigen presentation, a cellular process dependent on the efficient lysosomal digestion of internalized proteins by phagocytosis, and in the response to oxidative stress (Extended data 7a). Additionally, functional classes of biological functions associated with normal functions of pro-repair macrophages were also altered in Manf-deficient macrophages (Extended data 7a), suggesting functional alterations in the context of tissue repair.

To better characterize the alterations of Manf-deficient macrophages we zoomed in on the pro-repair population. The F4/80^{pos}Ly6C^{Low} subpopulation of pro-repair macrophages was isolated by FACS from Manf$^{Cx3cr1\Delta}$ and Manf^{Cx3cr1WT} muscles at 3dpi and analyzed by transmission electron microscopy (TEM). Manf-deficient pro-repair macrophages exhibited marked structural

differences (Fig. 6c-e and Extended data 8), characterized by a significant increase in size (p<0.0001, Fig. 6c) and an accumulation of large vesicular structures, often filled with undigested cellular material (Fig. 6d-e). These structural alterations are consistent with the gene expression changes associated with alterations in the lysosomal compartment and hydrolytic activity and may reflect alterations in the phagocytic pathway, previously associated with the phenotypic transition of macrophages into a pro-repair state[13].

To specifically test whether Manf-deficient macrophages showed defects in phagocytic activity we performed *in vitro* experiments using bone marrow-derived macrophages (BMDMs) generated from Manf[R26Δ] mice and measured their capacity to uptake opsonized beads and to increase their lysosomal hydrolytic activity upon stimulation with cellular debris. We could not detect any defects in cargo uptake capacity in MANF-deficient macrophages (Fig. 6f and Extended data 7b). However, while macrophages that express MANF increased their basal lysosomal hydrolytic activity by about 60% upon stimulation with cellular debris, MANF-deficient macrophages only increased their lysosomal activity by about 30%, evidencing significant (p=0.03) defects in phagocytosis-associated lysosomal hydrolysis (Fig. 6g-h).

Restoring MANF levels improves regeneration in ageing

To understand if similar defects were present in old animals, we performed RNAseq analysis of pro-repair macrophages (CD11b^{pos}F4/80^{pos}Ly6C[Low]) isolated from aged muscles at 3dpi. The dataset of up-regulated genes was enriched for gene ontologies associated with inflammatory activation, suggesting a shift in the gene expression profile of the pro-repair population towards a pro-inflammatory phenotype (Fig. 7a). Similarly to what we observed in MANF-deficient macrophages, the dataset of down-regulated genes revealed enrichment in gene ontologies of cellular components associated with lysosomal and endosomal compartments, but also changes associated with filopodia and lamellipodia, not present in MANF-deficient macrophages (Fig. 7b). Genes down-regulated in aged macrophages also classified in biological processes with relevance within the context of tissue regeneration, such as wound healing, endothelial cell morphogenesis or regulation of cell-cell adhesion (Extended data 9a). Interestingly, *in vitro* assays using BMDMs derived from yg and aged mice, showed that aged macrophages also manifest defective phagocytosis-induced lysosomal activity, which could be improved by rMANF supplementation (Fig. 7c and Extended data 9b).

Since MANF induction following injury was impaired in aged animals (Fig. 1c and Extended data Fig. 1b-c); defects in the repair-associated myeloid response and muscle regeneration were similar in aged and MANF-deficient mice (Fig. 1d-I and Fig. 2); and MANF supplementation was sufficient to restore pro-repair macrophages in models of MANF deficiency (Fig. 5c) and improve lysosomal activity in phagocytic aged macrophages (Fig. 7c), we sought to explore whether MANF therapy could allay the age-related defects in muscle regeneration. Our strategy consisted in delivering rMANF through daily intramuscular (i.m.) injections (2 or 4ug/ injections) starting at 1 dpi and up to the day of analysis (Fig. 7d). We found that delivery of rMANF to injured muscles of aged mice was sufficient to normalize the repair-associated myeloid response, restoring the numbers of myeloid cells and pro-repair macrophages at 3 dpi (Fig. 7e-g). The effects were dose-dependent and MANF therapy at 4ug/i.m. injection resulted in a complete rescue of the repair-

associated myeloid response. Importantly, the same regimen of MANF therapy improved muscle regeneration in aged animals, resulting in an increase in the CSA of new myofibres and a reduction in the accumulation of uncleared necrotic fibres (Fig. 7h-k). These data show that restoring MANF levels during regeneration in aged muscles is sufficient to normalize the repair-associated myeloid response and suggest that immune modulatory interventions that rejuvenate macrophage function can be used to improve the regenerative capacity of aged muscles.

Discussion

Age-related alterations in myeloid populations occur in the aged skeletal muscle, in homeostasis, with detrimental consequences for MuSC activity and tissue health[28-31]. However, the effects of ageing on the myeloid response associated with muscle regeneration have just started to be explored[31,32]. Here we uncovered a new regulator of the myeloid response to muscle injury, MANF, involved in the maintenance of a proper balance of macrophage populations throughout muscle regeneration. By identifying a critical down-regulation of MANF signalling in the aged regenerating skeletal muscle, we demonstrated how age-related changes in immune modulatory mechanisms contribute to the skeletal muscle's regenerative failure in ageing.

Previous studies have established that macrophages are essential for effective muscle repair, and murine models of macrophage ablation show defects in muscle regeneration characterized by accumulation of necrotic debris and defective myofiber formation[13,33], resembling the phenotype of MANF-deficient mice. The current knowledge regarding the role of macrophages on muscle regeneration is centred on the idea that macrophages act as signalling sources that control MuSC function, and intercellular communication defects are at the origin of muscle regenerative impairments in conditions of macrophage dysfunction[12]. There are indeed several macrophage-derived signals that affect MusC activity, many of which altered during regeneration in ageing, including Klotho[34,35], GDF3[32], CXCL10[36], osteopontin[37], among others[38]. However, beyond their signalling activity, macrophages perform a central function of cellular debris clearance in the context of tissue injury. Indeed, phagocytic activity was recently shown to be essential for the phenotypic transition between macrophage populations[13,39] and for effective muscle regeneration[39]. Interestingly, the accumulation of necrotic debris in regenerating MANF-deficient mice is accompanied by defects in macrophage phenotypic transition. Thus, our data linking MANF function with phagocytosis-induced lysosomal activity may be the underlying mechanism through which MANF-loss leads to impairments in macrophage balance. Even though age-related immune signalling alterations have been linked with regenerative failure in aging[31], it remains to be demonstrated whether re-establishing the immune cell function in aged animals is sufficient to improve regenerative capacity. Our results support the idea that direct modulation of macrophage function in ageing could be used to improve muscle regeneration.

We also observed defects in the accumulation of myeloid cells following muscle injury in aged and MANF-deficient mice that warrant further investigation. The simultaneous rebalancing of macrophage populations and re-establishment of myeloid numbers following MANF delivery during regeneration raises the intriguing prospect that the two defects are linked. One possibility is that pro-repair macrophages are necessary for the secretion of a signal that sustains continuous recruitment of myeloid cells, whereas another is that accumulated debris produces and inhibitory

signal that prevents further recruitment. Alternatively, considering its pleiotropic activities, it is possible that MANF may have an additional independent function, either local or systemic, not related to their direct activity in macrophages, which affects the efficiency of myeloid recruitment to the muscle.

MANF is an ubiquitous protein with multiple cellular targets reported[16,18]. Although initially identified as a neurotrophic factor with cytoprotective activity on dopaminergic neurons[40,41], MANF has since been associated with additional functions in the retina[15,42], heart[43,44], liver[20,45], pancreas[46] and inner ear[47], some of which in the context of aging[20,21,48]. Additionally, MANF's cytoprotective action now encompasses the engagement of tissue repair mechanisms through immune modulation[15,48-50]. Indeed, our data suggest that macrophages are the main source and target of MANF signaling during muscle repair. Our approach involved the use of two independent drivers, previously shown to be specific for macrophages in the muscle[51,52]. Nevertheless, the residual expression of MANF in macrophage depleted muscles, and the reduction in the magnitude of regenerative defects of our conditional $Manf^{Cx3cr1\Delta}$ relative to full $Manf^{26\Delta}$ model leave open the possibility of additional MANF sources in the regenerating muscle. Thus, the effects of a partial unspecific deletion of MANF in other cell types in our conditional models cannot be completely excluded and should be taken as a limitation of this study. In the future, it would be interesting to test whether MANF ablation in other cell types affects muscle regeneration. It is also possible that beyond macrophages, other cellular targets of MANF in the muscle affect regenerative success, including the myofibre. This could be mediated by the regulation of the ER stress response, a cellular process associated with MANF signaling in multiple cell types[53,54], and required in the myofibre to support MuSC activity during regeneration[55]. Alternatively, MANF could also act as a direct negative regulator of NFκB signaling in the myofibre[56], a mechanism previously implicated in the age-related loss of regenerative capacity[57].

Based on our assays, we propose that the effects we observe are mostly driven by an autocrine activity of MANF in macrophages. Addressing the question of whether blocking MANF response specifically in macrophages recapitulates the regenerative defects observed in our models is currently limited by our lack of knowledge regarding a MANF receptor in macrophages. Several possibilities can be explored to address this gap in knowledge: Neuroplastin has been proposed as a MANF receptor in other cell types, associated with the regulation of anti-inflammatory signaling[58]. Interestingly, a recent report uncovered a role of Neuroplastin in macrophages, in the context of infection, connected with phagocytosis associated lysosomal function and chemotaxis[59]. Additionally, co-localization of MANF and TLR receptors in innate immune cells has been observed in other model organisms[60] and may also be explored as a link between MANF function and phagocytic activity[61].

Our work supports the idea that loss of MANF-mediated immune modulation is one of the factors contributing to a decline in skeletal muscle regenerative capacity in aging. The use of immune modulatory adjuvants in regenerative medicine can be an attractive strategy to improve the clinical outcome of stem-cell based therapies in older adults[1]. The implementation of these therapeutic solutions is going to require a better understanding of the age-related impairments of immune mechanisms associated with tissue repair. From this work, MANF emerges as a potential candidate to be used in a clinical setting where MuSCs are applied to the aged skeletal muscle. However it is likely that other players are also involved in the process and an extended

characterization of the effects of aging on the regulation of the immune response to muscle injury is certainly going to be a central question of future research.

Methods

Animals

All mice used in these studies were housed at the DGAV accredited rodent facility of Instituto de Medicina Molecular, in individually ventilated cages within a specific and opportunistic pathogen-free (SPOF) facility, on a standard 12/12h light cycle. All the research reported in this study complied with relevant institutional and national animal welfare laws, guidelines and policies. The study protocol was reviewed and approved by iMM ORBEA and licensed by DGAV (DGAV Project License Number 022860 \2020).

Old wt C57BL/6 mice were purchased from Charles River, Europe with 18-20 months and further aged in house until analysis. Young wt mice were either purchased from Charles River, Europe; or born in house and generated using C57BL/6 breeders purchased from Charles River, Europe.

To create a mouse model allowing an inducible and ubiquitous ablation of *Manf* we generated Rosa26[CRE-ERT/+]Manf^{fl/fl} mice. Mice carrying the Rosa26[CRE-ERT] allele are B6;129-Gt(ROSA)26Sortm1(cre/ERT)Nat/J and were purchased from The Jackson Laboratory (JAX, stock no: 004847). In these mice a Cre[ERT] cassette is inserted within intron 1 of the GT(ROSA)26Sor locus and is expressed under the control of its endogenous promoter. Mice carrying the Manf[fl] allele were previously described[20]. Heterozygous carriers of the Cre[ERT] allele and homozygous carriers of the Manf[fl] allele were used for these studies. Cx3cr1[CRE-ER/+], Manf^{fl/fl} mice were previously described[20] and specificity of the driver in muscle tissue for macrophages is shown in REF[52]. To induce Cre activity, mice received daily intra-peritoneal injections of tamoxifen (T5648-1G – Sigma) in sterile corn oil, at a dose of 75mg/Kg of body weight. Control mice were littermates of the same genotype that received sham injections (corn oil) or Manf^{fl/fl} mice that received tamoxifen injections. To create a mouse model where MANF is ablated in macrophages in a tamoxifen-independent manner we generated LysM[CRE/+]/MANF^{fl/fl} mice. Mice carrying the LysM[CRE] allele are B6.129P2-Lyz2tm1(cre)Ifo/J and were purchased from JAX (stock number 004781). Heterozygous carriers of the Cre allele and homozygous carriers of the Manf[fl] allele were used for these studies. Control mice were MANF^{fl/fl} littermates without the Cre allele. Specificity of the Lyz2 driver in muscle tissue for macrophages is shown in REF[51]. LysM[CRE/+], Manf^{fl/fl}; Cx3cr1[CRE-ER/+], Manf^{fl/fl} mice; and MANF^{fl/fl} mice were generated at the Buck Institute for Research on Aging (Novato, CA, USA) and re-derived into SPOF C57BL/6J strain by *in vitro* fertilization. Primers used for genotyping all mouse strains are listed in Supplementary table 1. Male and female animals were used in the studies reported.

In vivo procedures in mice

All procedures involving animals were approved by Direção Geral da Alimentação e Veterinaria (DGAV) and performed at the rodent facility of Instituto de Medicina Molecular.

Induction of muscle regeneration: Regeneration of skeletal muscle was induced by intramuscular (i.m.) injection of sterile 1.2% Barium Chloride (Sigma: 342920) in saline solution (0.9% NaCl, B. BRAUN) into the tibialis anterior (TA, 40ul) or quadriceps (QC, 50ul) muscle of

the mice. At the designated time points after injury, mice were euthanized and muscles were collected for analysis. Animals were anesthetized for the procedure with Isoflurane inhalation. Tamoxifen injected mice were anesthetized with Ketamine 75mg/Kg of body weight + Medetomidine 1mg/Kg of body weight before i.m.injection.

Macrophage ablation: Chemical ablation of macrophages was performed using a clodronate-liposome solution. Clodronate-liposomes or PBS-liposomes (LIPOSOMA – Research solution SKU: CP-010-010) at 5mg/ml were inject intravenously (tail) at a dose of 100ul/10g of body weight. Animals received one injection on the day before injury, and then daily injections until analysis starting at 1dpi.

rMANF intramuscular injection: Injured mice received daily i.m. injections of 20ul of saline solution (0.9% NaCl, B. BRAUN) containing 2µg or 4µg of hrMANF protein (P-101-100, Icosagen), in the injured muscle starting at 1 dpi until the day of analysis. Control animals in the same experiment received the same regimen of i.m. injections of saline solution without rMANF supplementation. hrMANF protein used had less than 1EU of endotoxin per mg of protein. The use of hrMANF protein in murine studies has been validated in other studies[15,20,21,46].

In Vivo EdU (5-ethynyl-2'-deoxyuridine) Labeling: EdU labeling was performed by intraperitoneal injection of 200ul of EdU (3mg/ml) dissolved in PBS, 24h prior to analysis.

Histological analysis, imaging and quantification methods for muscle tissue

Muscle tissue harvesting and storage: Animals were euthanized and tissues were harvested. For histology analysis the dissected TA muscle was mounted vertically on a tragacanth gum (G1128-100G – Sigma) placed on a card board. The tissue was frozen in methyl-butane (VWRC103614T – VWR) cooled with liquid nitrogen, for about 13 to 17 seconds depending on muscle size and stored at -80ºC for further analysis as described[62]. Frozen tissue was cryosectioned at 10µm thickness on a cryostat (LEICA CM 3050S), collected on Superfrost microslides (VWR) and stored at -80ºC until analysis. Samples processed for RNA and protein analysis were flash frozen in cryotubes submerged in liquid nitrogen.

H&E staining of muscle sections: Muscle cryosections collected on slides were thawed at room temperature (RT) for 10min. Cryosections were placed in distilled water for 5min, stained on Harris Hematoxylin (05-06004E – Enzifarma), placed under running water for 5min, dipped on ethanol 70%, stained on eosin (HT110132-1L- Sigma). Stained tissue was serially dehydrated in 70%, 95% and 100% (twice) ethanol for 30 sec on each alcohol, incubated in xylene (3803665EGDG – Leica Microsystems) for at least 10 min and mounted with MICROMOUNT (3801731DG - Leica Microsystems).

Immunohistochemistry (IHC) of muscle cryosections and nuclei staining: Muscle cryosections collected on slides were thawed, permeabilized with PFA 4% in Phosphate-buffered saline (PBS) 10 min at RT, incubated in boiling 10mM Citrate buffer 45 min, blocked with Mouse on Mouse Blocking Reagent (R&D Systems) 2h and incubated with primary antibody, diluted in blocking solution, overnight (O/N) at 4°C. Primary antibody was washed 4x with PBS containing 0.1% Tween20 (PBS-T) and detected by incubating 2h30min with Alexa conjugated secondary

antibodies (Abcam). Secondary antibody was washed 5x with PBS-T. Nuclei were stained for 5min with 300nM DAPI (4',6-diamidino-2-phenylindole) in PBS at RT. Slides were rinsed in PBS and mounted with Mowiol mounting media and microscope cover glass No. 1.5H (Marienfeld). Co-staining of F4/80 and MANF was performed without the permeabilization with Citrate buffer and blocked with Horse Serum (HS) 10% in PBS-T. Staining of necrotic myofibres using secondary antibody anti-mouse IgG coupled to Alexa-647 was performed without primary antibody incubation overnight. As myofibers become permeable during necrosis, the passive uptake of IgG proteins allows for staining of necrotic fibers using anti-IgG antibodies[63]. For information on primary antibodies used see Supplementary Table 2.

Imaging: Digital images were acquired at the Bioimaging and Comparative Pathology facilites of Instituto de Medicina Molecular using: (1) a digital slide scanner NanoZoomer SQ (HAMAMATSU), with an objective of 20X magnification, for H&E stained sections; (2) a motorized inverted widefield fluorescence microscope (Zeiss) equipped with CCD camera (Photometrics CoolSNAP HQ CCD), with a 20X objective for IHC stained sections (eMHC, IgG). The total stained sections after imaging were reconstructed through image overlay (10%); (3) a Zeiss LSM 710 confocal laser scanning microscope (F4/80/MANF IHC). Metamorph 7.7.9.0 was used for image acquisition on Zeiss Axiovert 200M. ZEN 2012 SP5 FP3 (black) was used for image acquisition on Zeiss LSM 710.

Image quantification: To assess the effectiveness of the muscle regeneration the individual new myofibres (eMHC[pos]) were manually outlined in the total muscle section and their cross-sectional area (CSA) was determined with the public domain image analysis software Image J 1.51j8 or 1.53t. The number of necrotic fibres in total muscle section was quantified using the same software.

Flow cytometry (FC) analysis

Muscle cell population analysis: To obtain single cell suspensions, muscles were mechanically disaggregated and dissociated in DMEM 1% P/S media containing collagenase B (Roche) 0.2% and Calcium dichloride ($CaCl_2$) 0.5 mM at 37 °C for 1h and then filtered through 70 µm cell strainers (Falcon). Cells were incubated in 1x Red Blood Cell (RBC) lysis buffer (Santa Cruz Biotechnology) for 10 min on ice, resuspended in 1ml of DMEM 10% FBS 1% P/S media and counted. For flow cytometry analysis (FC analysis), single cell suspension samples were resuspended in PBS containing 5% HS with fluorophore-conjugated antibodies at a density of $1x10^6$ cells/100 µl, incubating 30 min at 4ºC, protected from light. Cells were re-suspended in PBS containing 5% HS for FC analysis. For information on antibodies used see Supplementary Table 3. CD45, CD31 markers were used to exclude the Lin (-) negative population from single live cell population and the population of MuSCs and FAPS were identified as α7-integrin[pos] and Sca-1^{pos}, respectively. Live cells were identified using LIVE/DEAD™ FixableNear-IR Dead Cell Stain (Invitrogen). Gating strategy used in FC analysis of CD45^{pos} immune cell population, endothelial cells, FAPS and MuSCs is shown in Extended data Figure 2a. Gating strategy used in FC analysis of myeloid cells (CD11b^{pos}), pro-repair macrophages (F4/80^{pos}Ly6C[Low]), pro-inflammatory macrophages (Ly6C[High]), and neutrophils (Ly6G^{pos}) is presented in Extended data Figure 2d.

Proliferation analysis: Cell proliferation was determined by EdU detection using the EdU-Click 488 kit. Following staining of cell-surface antigens with antibodies as described above and cell fixation using 1x Intracellular Fixation Buffer (eBioscience™, 00-8222-49) in PBS containing 5% HS, cell suspensions were permeabilized in 100ul of 1x Permeabilization Buffer (eBioscience™, 00-8333) in distilled water. Cells were incubated in a Click reaction for 30 min at RT protected from light, washed with 500ul of Permeabilization buffer, resuspended in PBS containing 5% HS and immediately analyzed by FC. FMO control for EdU Detection was obtained using all the components for the click reaction except for the dye 6-FAM-Azyde.

Apoptosis analysis: Cell apoptosis was monitored by staining the cells with Apopxin Green solution from the Apoptosis/Necrosis Assay Kit (ab176749). Following the staining of cell-surface antigens with antibodies as described above, cells were resuspended in Assay Buffer with Apopxin Green Indicator at 1:100 and incubated for 45 min at RT. Apopxin Green Solution was not added to cells for FMO control.

Blood cell population analysis: Blood was collected by heart puncture and incubated twice in 1x RBC lysis buffer for 15 min at RT, with periodic inversions. Blood cells were incubated in viability dye Zombie Aqua (1:1000; Biolegend) diluted in PBS for 15 min on ice, blocked using anti-mouse CD16/32 FcγR (Biolegend) diluted at 1:250 in 1x Brilliant Stain Buffer Plus (BD Biosciences) in PBS-2% FBS (BV Buffer) for 15 min, and fluorophore-conjugated antibodies were added at a density of 5×10^5 cells/50 µL, incubated for 30 min at 4°C, and protected from light. Blood cells were resuspended in PBS containing 2% FBS for FC analysis. For information on the antibodies used, see Supplementary Table 3. Live blood cells were identified using the viability dye Zombie Aqua. The gating strategy used in FC analysis of neutrophils (Ly6G^{pos}), Ly6C^{neg} monocytes (Ly6C^{neg}Cx3cr1^{pos}), and Ly6C^{pos} monocytes is presented in Extended Data Figure 5g.

For all analyses, characterization of cell populations was performed at the Flow cytometry facility of Instituto de Medicina Molecular, using a cell analyzer LSRFortessa X-20 (BD Bioscience) with FACSDiva 8.0 software. Flow cytometry data were analyzed using FlowJo (BD Biosciences) analysis software.

Fluorescence activated cell sorting (FACS) of macrophage populations

Single cell suspensions, obtained as described above, were used to isolate macrophage populations through staining with fluorochrome-conjugated antibodies presented in Supplementary Table 3. CD45^{pos} F4/80^{pos} macrophages were selected from the viable cells present in the single cell suspension. F4/80^{pos}Ly6C^{Low} and LyC6^{High} macrophages were isolated using the gating strategy presented in Extended data Figure 2d. The isolation of pure populations of cells was performed at the Flow cytometry facility of Instituto de Medicina Molecular using a FACSAria IIu (BD Bioscience) or a FACSAria III (BD Bioscience) using the software FACSDiva 6.1.3. Cells were collected in PBS containing 5% HS and used either for protein extraction, RNA extraction, TEM analysis or *ex-vivo* assays.

Ex-vivo macrophage analysis

Whole muscle single cell suspensions: Single cell suspensions of 2pi injured muscles were obtained as described above. For each animal, 500 000 cells were collected at 0h or cultured and collected after 16h. Cells were incubated in suspension at 37ºC in SF medium (Corning® SF Medium, with L-glutamine and 1 g/L BSA) supplemented with 10% FBS and 1% Pen/Strep. In conditions of MANF supplementation, rMANF (P-101-100, Icosagen) was used at a concentration of 10µg/ml. Cells collected at 0h and 16h were stained for FC analysis of muscle immune populations as described above.

Sorted Ly6C^{High} macrophages: Ly6C^{High} macrophages were isolated by FACS from 2dpi injured muscles, as described above, and 50.000 cells were collected for analysis at 0h or cultured and collected for analysis after 16h. Cells were incubated at 37ºC in DMEM medium supplemented with 10% FBS and 1% Pen/Strep. Cells collected at 0h and 16h were stained for flow cytometry analysis of muscle immune populations or used for RNA analysis. Ly6C-APC antibody was used during cell sorting and Ly6C-FITC antibody was used for detection of Ly6C at 0h and 16h in flow cytometry analysis.

Transmission Electron Microscopy analysis of macrophages

Sample processing and imaging: Pro-repair macrophages were isolated by FACS as described above, plated on 12 mm coverslips inserted in a 24-well plate with DMEM media containing 1% PS and 10%FBS, and allowed to adhere for 2h. Sample processing and imaging was performed at the Electron Microscopy facility at Instituto Gulbenkian de Ciênca (IGC, Lisbon, Portugal). Cells were fixed with 2% formaldehyde (FA) - 2.5% Glutaraldehyde in 0.1M phosphate buffer (PB) for 45min on ice and then fixed O/N in 1% FA in PB at 4ºC. The following day, cells were washed 2x in PB, post-fixed with 1% osmium in PB for 1h on ice, washed 2x in PB, 2x in water, stained with 1% tannic acid 20min on ice, washed 2x in water, stained with 0.5% in Uranyl acetate 1h at RT and serial dehydrated in increasing concentrations of ethanol. Coverslips with cells were mounted on top of EPON capsules and baked at 60ºC O/N. Sections of 70 nm were obtained using a UC7 Ultramicrotome (Leica) and stained with uranyl acetate and lead citrate for 5 minutes each. Images of single macrophages were acquired on a Tecnai G2 Spirit BioTWIN Transmission Electron Microscope (TEM) from FEI operating at 120 keV and equipped with an Olympus-SIS Veleta CCD Camera.

Image quantifications: Quantification of individual pro-repair macrophages from Manf$^{Cx3cr1\Delta}$ (n=42) and Manf^{Cx3cr1WT} (n=54) mice, analyzed by TEM, was performed using the ImageJ software, after scale normalization. Intracellular vesicles were manually surrounded, and the number and area were determined. In addition, the area of each cell was also calculated.

In vitro experiments with bone marrow-derived macrophages (BMDMs)

Preparation of BMDMs: BMDMs were differentiated *in vitro* from bone marrow (BM) progenitors. To isolate BM, both hindlimbs of each mouse were collected and the femur and tibia were individualized and kept on ice in sterile PBS with 1%P/S. Bone marrow was flushed out onto a plate using a 1ml syringe with a 26G needle filled with sterile media DMEM 10%FBS 1%P/S. Red blood cell clumps were mechanically disrupted using the syringe, and the cell suspension was collected and filtered through a 70µm filter, centrifuged at 500g for 5 minutes, resuspended in 1

ml of 1x RBC lysis buffer and incubated at RT for 5 minutes and washed with 10 ml of PBS. Cells were diluted in complete media to achieve 10^6 cells/ml density and plated in 10cm plates. Plated cells were supplemented with CSF-1 at 50ng/ml (Biolegend) and cultured at 37ºC. On the third day, media was changed and re-supplemented with CFS-1. On the sixth day, cells were detached and frozen in FBS 10%DMSO.

Preparation of Apop-necro: For Apop-Necro debris preparation, C2C12 myoblast cell line was used (ATCC, CRL1772). C2C12 cultures at 80% confluence were starved in PBS overnight to induce cells apoptosis. The following day, PBS and apoptotic cells in suspension were collected and counted. C2C12 suspension was centrifuged for 5min at 3000G. Pellet was then frozen and stored at -80ºC until BMDM stimulation.

Lysosomal-activity assay in BMDMs: BMDMs were thawed and 200.000 cells were plated in 12 well plates in medium supplemented with 10% FBS and 1% Pen/Strep and incubated overnight at 37ºC, in the absence of CSF-1. Lysosomal intracellular activity was evaluated using the Lysosomal Intracellular Activity Assay Kit (Abcam, ab234622). For the assay, cells were incubated with a self-quenched substrate in DMEM supplemented with 0.5% FBS and 1% Pen/Strep for 3h, according to manufactures' instructions. Basal activity was accessed in the absence of any co-stimulation. Phagocytosis-associated lysosomal activity was assessed during co-stimulation with apop-necro debris at a proportion of 2:1. Frozen apoptotic cells were thawed immediately before stimulation to induce additional necrosis. Bafilomycin A was used as a control to inhibit lyosomal activity in both conditions. In conditions of MANF supplementation, rMANF (P-101-100, Icosagen) was used at a concentration of 10µg/ml during the assay. Lysosomal hydrolysis of the self-quenched substrate was measured by flow cytometry through the quantification of fluorescence intensity in the FITC channel.

Bead phagocytosis assays in BMDMs: BMDMs were thawed and 100.000 cells were plated in 24 well plates in medium supplemented with 10% FBS and 1% Pen/Strep and incubated overnight at 37ºC, in the absence of CSF-1. Evaluation of phagocytic uptake capacity was performed using Fluoresbrite® 641 Carboxylate Microspheres (Polysciences, 17797-1). Opsonization of the particles was performed by incubation in 50% FBS in PBS for 30min at 37ºC. Opsonized particles were added to the BMDMS at a concentration of 5×10^8/ml and incubated for 3h. Phagocytic uptake was measured by flow cytometry through the quantification of fluorescence intensity of the Fluoresbrite® 641 within the BMDM single cell population.

Protein analysis

Preparation of muscle protein extracts: Whole muscle samples, or cells obtained from FACS, were homogenized in Lysis buffer (50 mM Tris pH 7.5, 150 mM NaCl, 0.5% NP-40, 5 mM EDTA, 1%Triton, in Mili-Q water) supplemented with protease inhibitors and phosphatase inhibitors (Sigma) for 45 min or 20 min at 4ºC, respectively. The supernatant protein extracts were recovered by centrifugation and protein concentration in samples was determined using Bradford Reagent (VWR).

Western blot: Western blot analyses were performed on 12% SDS-PAGE. After electrophoretic separation, proteins were transferred onto nitrocellulose membranes using a Trans Blot Turbo

Transfer system (BioRad). Membranes were blocked with Tris-buffered saline-0.1% Tween 20 (TBS-T) containing 5% milk for 1h and incubated overnight at 4ºC with primary antibodies. Membranes were then incubated 1h with a peroxidase-conjugated secondary antibody (1:10000; Abcam), and developed using Pierce ECL Western blotting substrate (ThermoScientific) or Clarity™ Western ECL Substrate (BioRad). For information on primary antibodies used see Supplementary Table 4. Ponceau S solution (Sigma) was applied to the nitrocellulose membranes before the blocking step to assess the total protein present.

Enzyme-Linked Immunosorbent Assay (ELISA): MANF concentrations in muscle tissue samples were quantified using an in-lab mouse MANF (mMANF) ELISA[64]. mMANF ELISA recognized both mouse and human MANF but did not recognize MANF homolog CDNF or give signal from tissue lysates from Manf-/- mice, indicating that it was specific for MANF. Dynamic range of mMANF ELISA was 62.5 – 1000 pg/ml and its sensitivity 29 pg/ml. For mMANF ELISA measurement, muscle lysates from young mice were diluted at 1:500 in blocking buffer (1% casein in PBS-0.05% Tween-20), and lysates from young and old mice (2dpi, 3dpi) at 1:200, respectively. Recombinant human MANF (P-101–100; Icosagen) was used as a standard. All samples were measured in duplicate.

RNA analysis

Preparation of RNA samples: Total RNA from frozen muscle samples was extracted using TRIzol (Invitrogen), according to the supplier's instructions. Total RNA from sorted cells was extracted using RNeasy Micro kit (Qiagen), according to the supplier's instructions.

Reverse Transcription and real-time qPCR (RT-qPCR): Complementary DNA (cDNA) was synthesized using iScript cDNA synthesis kit (BioRad). Real-time PCR was performed on ViiA 7 Real-Time PCR System (Thermofisher Scientific), using Powerup SYBR Green MASTER MIX (Applied Biosystems). Expression of specific genes in each sample was normalized to beta-actin and results are shown as gene expression levels relative to levels in control samples which are arbitrarily set to one. For information on primer sequences see Supplementary Table 5.

RNA sequencing and bioinformatics analysis: Library preparation, RNA sequencing, read mapping and FPKM quantification was performed as a service at Novogene (Cambrige, UK). RNA samples prepared as described above, from sorted macrophages (Manf$^{Cx3cr1\Delta}$ vs Manf^{Cx3cr1WT}) or pro-repair macrophages (Yg vs. old) were shipped to Novogene. Novogene team was responsible for Illumina library preparation (poly A enrichment) and sequencing using a NovaSeq instrument to generate 150 bp pair-end reads with an output of 6G per sample. Gene Ontology and KEGG analysis was carried out using The Database for Annotation, Visualization and Integrated Discovery (DAVID, https://david.ncifcrf.gov/, ref. 76).

Statistics & Reproducibility

For the experiments reported in this study a minimum of 3 independently manipulated animals were used per condition. In the graphs reporting data collected from animals, each dot corresponds to an independent measurement from an independent animal.

For experiments reporting data in BMDMs (Fig. 6f-h and Extended Data 6f), each dot in the graph corresponds to an independent measurement from an independent assay in a culture of BMDMs generated from an independent animal.

For experiments reporting *ex vivo* assays (Fig. 5), each dot in the graph corresponds to an independent measurement from an independent assay in a culture generated from an independent animal.

For experiments involving EM analysis (Fig. 6c-e and Extended data Fig. 8), macrophages were sorted from n=3 animals/condition in 2 independent experiments (experiment 1: n=1/condition; experiment 2: n=2/condition, pooled). Samples obtained in each experiment were processed independently for analysis.

For experiments involving rMANF supplementation in culture (Fig. 5c and 7c), the rMANF supplementation was compared to the control condition in the same source culture obtained from the same animal.

No statistical methods were used to pre-determine sample sizes, but our sample sizes are similar to those reported in previous publications[31]. No randomization method was used to allocate animals to experimental groups. Data collection and analysis were not performed blind to the conditions of the experiments. No data were excluded from the analyses.

All data are presented as average and standard error of the mean (s.e.m.). Statistical analysis was carried out using GraphPad Prism 5. For comparisons between two groups, a two-tailed Student's t test was used to determine statistical significance, assuming normal distribution and equal variance (not formally tested). For multiple comparisons, one-way ANOVA with Bonferroni's multiple comparison post-test or one-way ANOVA with Dunnett's multiple comparison post-test (Fig. 7, using the old groups as control for comparison) were used to determine statistical significance.

Data Availability

All the data generated or analysed during this study are included in the published article and its Supplementary Information and source data files, and are available from the corresponding author upon reasonable request. RNA-sequencing data generated in this study are available under accession numbers GSE224982 and GSE224983 on the NCBI Gene Expression Omnibus database. Correspondence and requests for materials should be addressed to P.S.-V., and J.N.

Acknowlegements

Author Contribuitions Statement

JN and PSV conceived the study, designed experiments, analyzed and interpreted data and wrote the manuscript. NSS and MFB designed and performed experiments, analyzed and interpreted data. IBA performed experiments and analyzed data. PL performed the ELISA analysis of muscle extracts. All authors revised the manuscript.

Competing Interests Statement

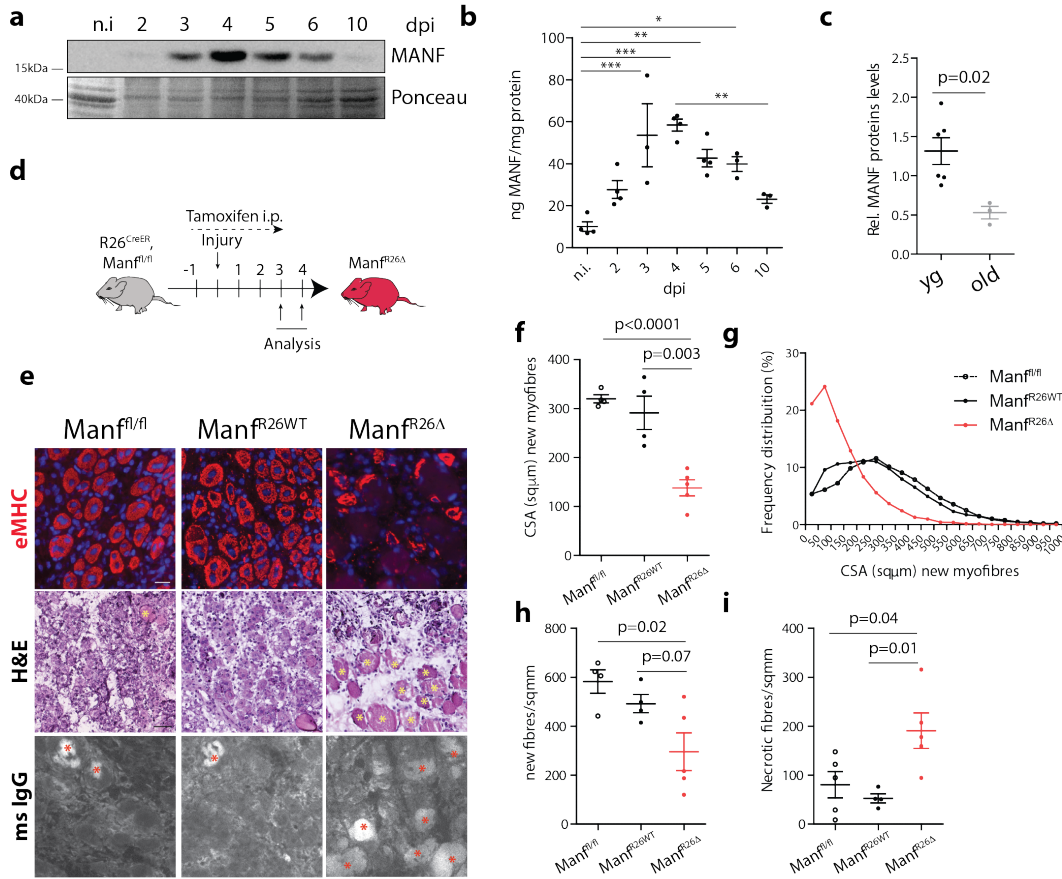The authors declare no competing interests.

Figure 1. MANF is essential for skeletal muscle regeneration

a, Western blot analysis of MANF levels in protein extracts of tibialis anterior (TA) muscles from yg wild type (wt, C57BL/6) mice, non-injured and at different time points following injury (2, 3, 4, 5, 6, 10 dpi). Ponceau S-staining of the membrane was used to verify equal protein loading in each sample. **b,** MANF protein levels, quantified by ELISA, in extracts of TA muscles from yg wt (C57BL/6) mice at different time points following injury (n=3 for 3,6,10dpi; n=4 for n.i,2,4,5dpi). **c,** Quantification of relative average levels of MANF, normalized to Ponceau levels, in protein extracts of TA muscles of yg (2-6mo) and old (22-25mo) wt (C57BL/6) mice at 3dpi (n=6, yg, n=3 old, see Extended data Fig. 1b for representative Western blot images). **d,** Experimental timeline for analysis of animals with inducible and ubiquitous ablation of MANF. **e,** Representative images of cryosections from TA muscles of Manf^{fl/fl}, Manf[R26WT] and Manf[R26Δ] mice, at 4 dpi, stained with eMHC (red, top, DAPI is used to identify nuclei, scale bar: 20μm), H&E (middle, scale bar: 50μm) and mouse IgG (bottom, scale bar: 20μm). Asterisks indicate necrotic myofibers. Quantifications of these stainings, for independent animals, are shown in Fig. 1f-i. **f-h,** Quantification of the average cross-sectional area of eMHC[pos] myofibres (f), frequency distribution of new myofibres by size (g) and density of new myofibres (h) in regenerating TA muscles from Manf^{fl/fl}, Manf[R26WT] and Manf[R26Δ] mice at 4dpi (n=4 for Manf^{fl/fl}, Manf[R26WT]; n=5 for Manf[R26Δ]). **i,** Quantification of the number of necrotic fibres in regenerating TA muscles from Manf^{fl/fl}, Manf[R26WT] and Manf[R26Δ] mice at 4dpi (n=4 for Manf[R26WT]; n=5 for Manf^{fl/fl}, Manf[R26Δ]). Data are represented as average ± s.e.m

and each n represents one animal. In b, p values are from one-way ANOVA with Bonferroni's multiple comparison post-test. In all other graphs, p values are from two-tailed Student's t-test. yg, young; n.i., non-injured; dpi, days post-injury; i.p., intraperitoneal; eMHC; embryonic myosin heavy chain; H&E, Hematoxylin and Eosin; msIgG, mouse Immunoglobulin; CSA, cross-sectional area.
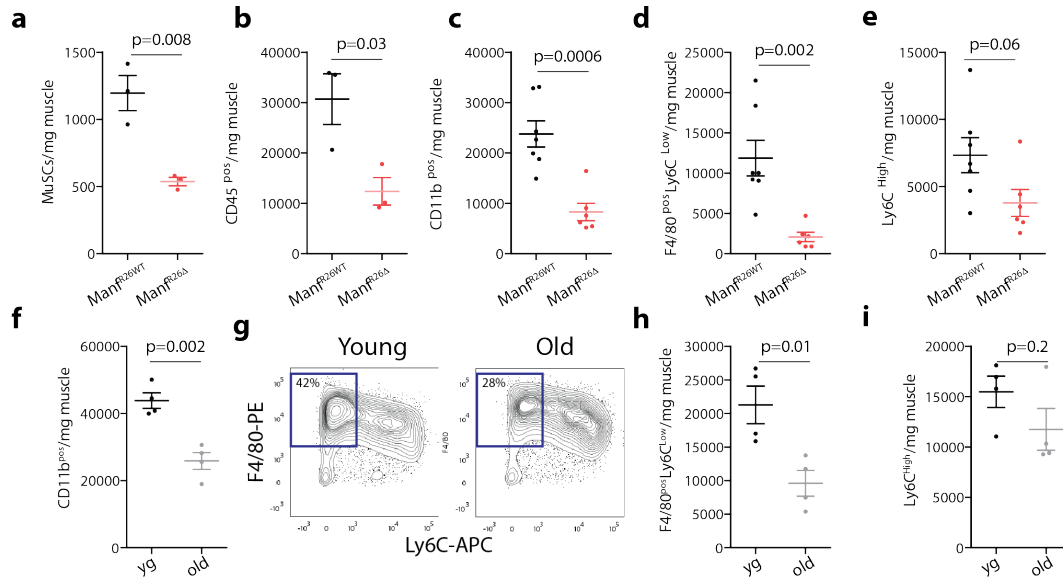
Figure 2

Figure 2. Aging and MANF-deficiency affect the myeloid response during muscle regeneration

a-e, Quantification, by flow cytometry, of MuSCs (a), CD45^{pos} immune cells (b), myeloid cells (CD11b^{pos}, c), pro-repair macrophages (F4/80^{pos}Ly6C^{Low}, d) and pro-inflammatory macrophages (Ly6C^{High}, e) in regenerating quadriceps (QC) muscles of Manf^{R26WT} and Manf$^{R26\Delta}$ mice at 3dpi (in a and b, n=3/condition; in c, d and e, n=7 for Manf^{R26WT}; n=6 for Manf$^{R26\Delta}$). **f,h,i,** Quantification, by flow cytometry, of myeloid cells (CD11b^{pos}, f), pro-repair macrophages (F4/80^{pos}Ly6C^{Low}, h) and pro-inflammatory macrophages (Ly6C^{High}, i) in regenerating QC muscles of yg (2-6mo) and old (22-24mo) wt (C57BL/6) mice at 3dpi (n=4/age). **g,** Representative density plots from flow cytometry analysis of muscle cell populations from yg and old animals based on F4/80 and Ly6C cell surface markers, at 3dpi. Percent numbers indicate pro-repair macrophages (F4/80^{pos}Ly6C^{Low}) relative to the CD11b^{pos} total population. Data are represented as average ± s.e.m and each n represents one animal. p values are from two-tailed Student's t-test. dpi, days post-injury; MuSCs; Muscle Stem Cells; yg, young.
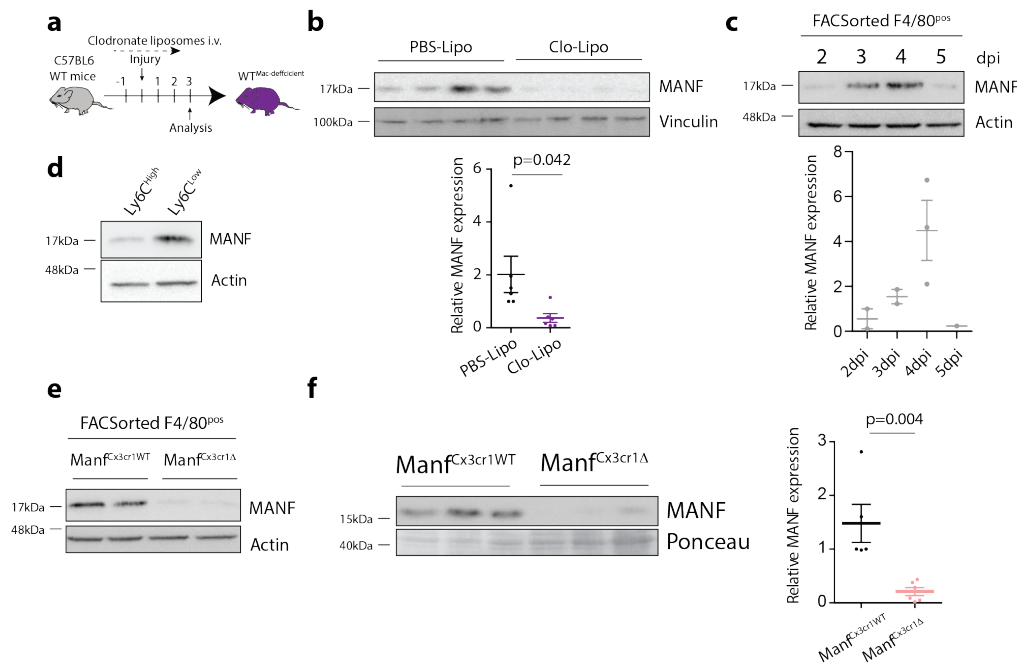
Figure 3

Figure 3. MANF is expressed in pro-repair macrophages

a, Experimental timeline for analysis of animals treated with clodronate liposomes. **b,** Western blot analysis of MANF levels in protein extracts of QC muscles from wt (C57BL/6) mice, at 3dpi, treated with clodronate liposomes (or control PBS liposomes). Quantification of relative average levels of MANF, normalized to Vinculin, is represented for each condition (n=6/condition). **c,** Western blot analysis of MANF levels in protein extracts from F4/80^{pos} cells FACS-isolated from QC muscles at different time points following injury. Quantification of relative average levels of MANF, normalized to Actin, is represented for each time-point (n=2 for 2,3dpi; n=3, 4dpi; n=1 (pooled from 4 mice), 5dpi). **d,** Western blot analysis of MANF levels in protein extracts from macrophage subpopulations (Ly6C^{High} and Ly6C^{Low}) FACS-isolated from QC muscles of wt mice, at 3dpi. Actin was used to verify equal protein loading in each sample. **e,** Western blot analysis of MANF levels in protein extracts from F4/80^{pos} cells FACS-isolated from QC muscles of Manf^{Cx3cr1WT} and Manf$^{Cx3cr1\Delta}$ mice at 3dpi. Actin was used to verify equal protein loading in each sample. **f,** Western blot analysis of MANF levels in protein extracts from muscles of Manf^{Cx3cr1WT} and Manf$^{Cx3cr1\Delta}$ mice at 3dpi. Quantification of average relative levels of MANF, normalized to Ponceau S-staining, are represented for each condition (n=5 for of Manf^{Cx3cr1WT}; n=6 for Manf$^{Cx3cr1\Delta}$). Data are represented as average ± s.e.m. and each n represents one animal. p values are from two-tailed Student's t-test. dpi, days post-injury; i.v., intravenous injection; PBS-Lipo, PBS Liposomes; Clo-Lipo, Clodronate Liposomes; FACS, Fluorescence activated cell sorting.
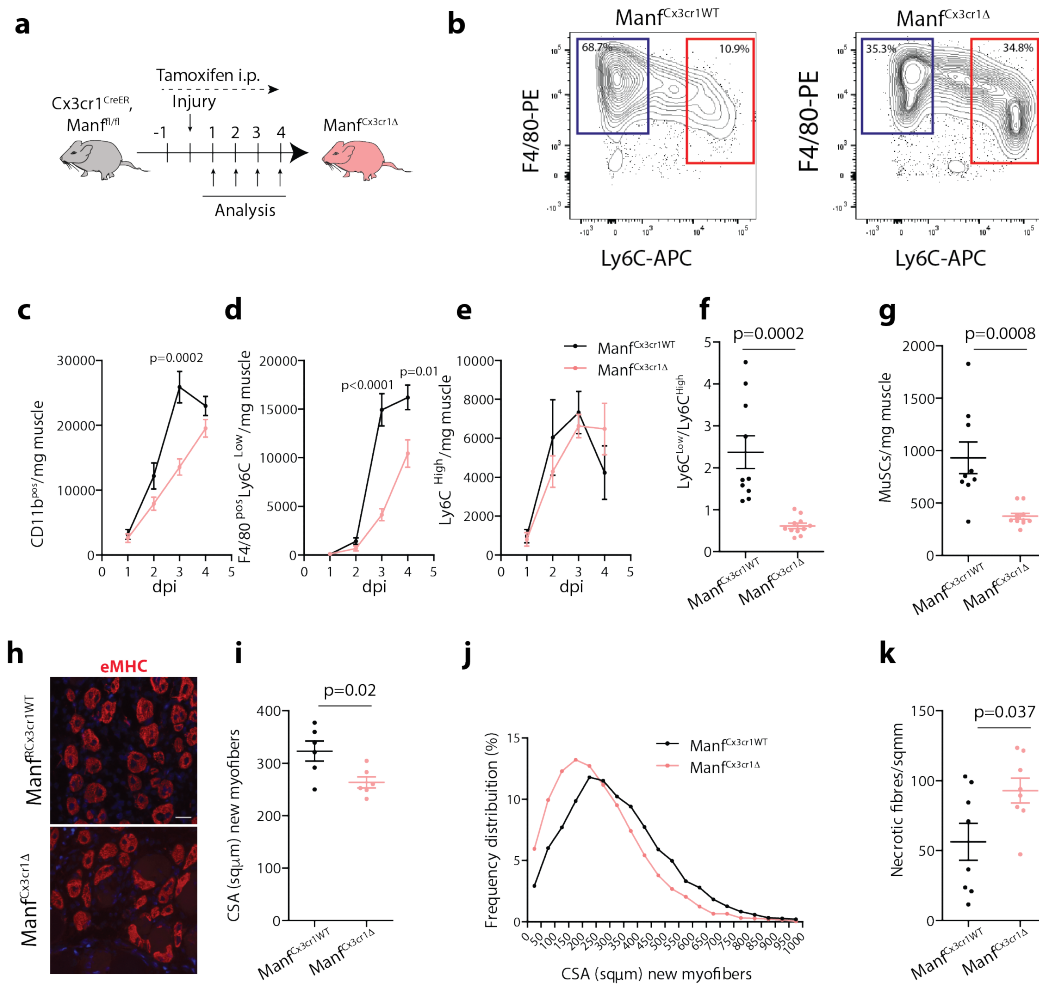
Figure 4

Figure 4. MANF derived from pro-repair macrophages is essential for skeletal muscle regeneration

a, Experimental timeline for analysis of animals with conditional ablation of MANF in Cx3cr1-expressing macrophages. **b,** Representative density plots from flow cytometry analysis of muscle cell populations from Manf^{Cx3cr1WT} and Manf$^{Cx3cr1\Delta}$ animals based on F4/80 and Ly6C cell surface markers, at 3dpi. Percent numbers indicate pro-repair macrophages (blue gate, F4/80^{pos}Ly6C^{Low}) and pro-inflammatory macrophages (red gate, Ly6C^{High}) relative to the CD11b^{pos} total population. **c-e,** Quantification, by flow cytometry, of myeloid cells (CD11b^{pos}, c), pro-repair macrophages (F4/80^{pos}Ly6C^{Low}, d) and pro-inflammatory macrophages (Ly6C^{High}, e) in regenerating quadriceps (QC) muscles of Manf^{Cx3cr1WT} and Manf$^{Cx3cr1\Delta}$ mice at different time points following injury (n=5 for Manf^{Cx3cr1WT} 2dpi; n= 7 for Manf$^{Cx3cr1\Delta}$ 4dpi; n= 10 for Manf^{Cx3cr1WT} 3dpi; n=11 for Manf$^{Cx3cr1\Delta}$ 3dpi; n=6 for all other conditions). **f,** Ratio of pro-repair to pro-inflammatory macrophages in regenerating QC muscles of Manf^{Cx3cr1WT} and Manf$^{Cx3cr1\Delta}$ at 3dpi (n= 10 for Manf^{Cx3cr1WT} 3dpi; n=11 for Manf$^{Cx3cr1\Delta}$ 3dpi). **g,** Quantification, by flow cytometry, of MuSCs in regenerating QC muscles of Manf^{Cx3cr1WT} and Manf$^{Cx3cr1\Delta}$ mice at 3dpi (n= 9 for Manf^{Cx3cr1WT} 3dpi; n=11 for Manf$^{Cx3cr1\Delta}$ 3dpi). **h,** Representative images of eMHC (red) staining in cryosections of regenerating tibialis anterior

(TA) muscle from Manf^{Cx3cr1WT} and Manf$^{Cx3cr1\Delta}$ mice, at 4dpi. DAPI is used to identify nuclei. Scale bar: 20μm. Quantifications of this staining, for independent animals, are shown in Fig. 2i-j. **i-j,** Quantification of the average cross-sectional area of eMHC^{pos} myofibres (i) and frequency distribution of new myofibres by size (j), in regenerating TA muscles from Manf^{Cx3cr1WT} and Manf$^{Cx3cr1\Delta}$ mice at 4dpi (n=6/condition). **k,** Quantification of the number of necrotic fibres in regenerating TA muscles from Manf^{Cx3cr1WT} and Manf$^{Cx3cr1\Delta}$ mice at 4dpi (n=8/condition, see Extended data Fig. 4d for representative images). Data are represented as average ± s.e.m. and each n represents one animal. p values are from two-tailed Student's t-test. dpi, days post-injury; i.p., intraperitoneal injection; eMHC; embryonic myosin heavy chain; CSA, cross-sectional area; MuSCs, muscle stem cells.
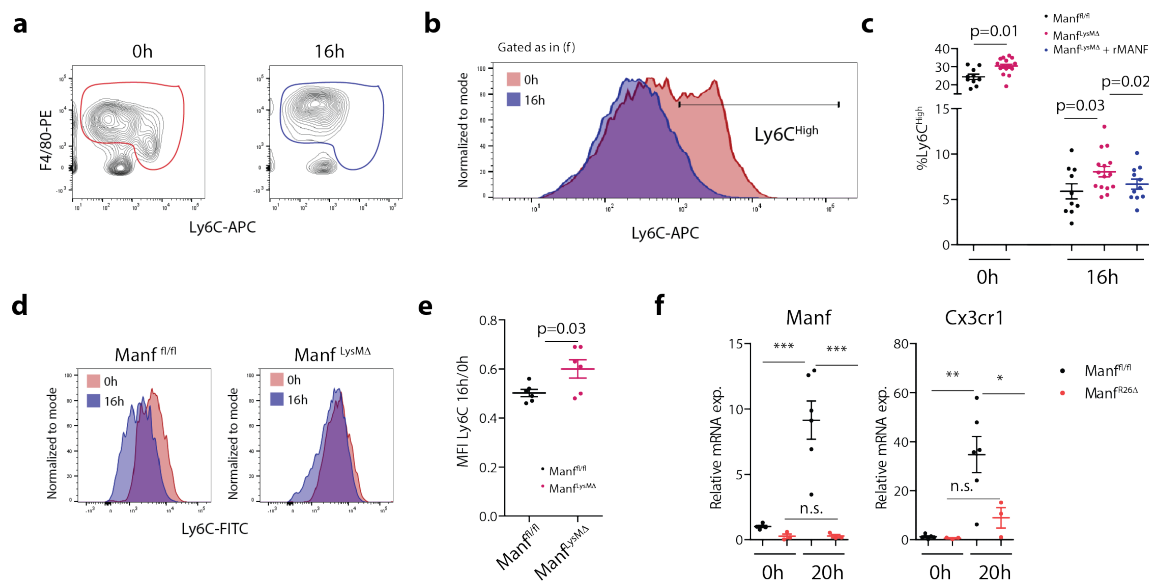

Figure 5

Figure 5. MANF-deficient macrophages have a delayed phenotypic transition

a, Representative density plots from flow cytometry analysis of muscle cell populations based on F4/80 and Ly6C cell surface markers after gating on the CD11b^{pos} population, for single cell suspensions isolated from quadriceps (QC) muscles at 2dpi, 0h and 16h after culture. Gates in red and blue define the population of monocytes/macrophages followed during the ex-vivo assays. **b,** Representative histogram of the Ly6C signal distribution on the monocyte/macrophage population, gated as in (a), in single cell suspensions isolated from QC muscles at 2dpi, 0h (pink) and 16h (blue) after culture. Ly6C^{High} gate is defined based on peak distribution at 0h, when both populations can be discriminated. **c,** Percentage of pro-inflammatory (Ly6C^{High}) macrophages, quantified by flow cytometry, in single cells suspensions isolated from QC muscles of Manf$^{fl/fl}$ and Manf$^{LysM\Delta}$ mice at 2dpi, 0h and 16h after culture, with or without recombinant MANF supplementation (n=10 for Manf$^{fl/fl}$; n=15 for Manf$^{LysM\Delta}$; n=11 for Manf$^{LysM\Delta}$ + rMANF). **d,**

Representative histogram of the Ly6C-FITC signal distribution on a population of macrophages isolated as Ly6C^{High} from QC muscles of Manf$^{fl/fl}$ and Manf$^{LysM\Delta}$ mice at 2dpi, 0h (pink) and 16h (blue) after culture. **e,** MFI in the Ly6C-FITC channel, quantified by flow cytometry, in Ly6C^{High} macrophages FACSorted from QC muscles of Manf$^{fl/fl}$ and Manf$^{LysM\Delta}$ mice at 2dpi, 0h and 16h after culture (n= 6/condition). **f,** Relative levels of Manf and Cx3cr1 mRNA, detected by RT-qPCR, in Ly6C^{High} macrophages FACSorted from QC muscles of Manf$^{fl/fl}$ and Manf$^{R26\Delta}$ mice at 2dpi, 0h and 20h after culture (n= 3 for Manf$^{R26\Delta}$; n=5 for Manf$^{fl/fl}$ 0h and n=6 for Manf$^{fl/fl}$ 20h). Data are represented as average ± s.e.m. and each n represents one animal. In f, p values are from one-way ANOVA with Bonferroni's multiple comparison post-test. For all other graphs, p values are from two-tailed Student's t-test. dpi, days post-injury; rMANF; recombinant Mesencephalic astrocyte-derived neurotrophic factor; MFI, Mean Fluorescence intensity. FACS, Fluorescence activated cell sorting.
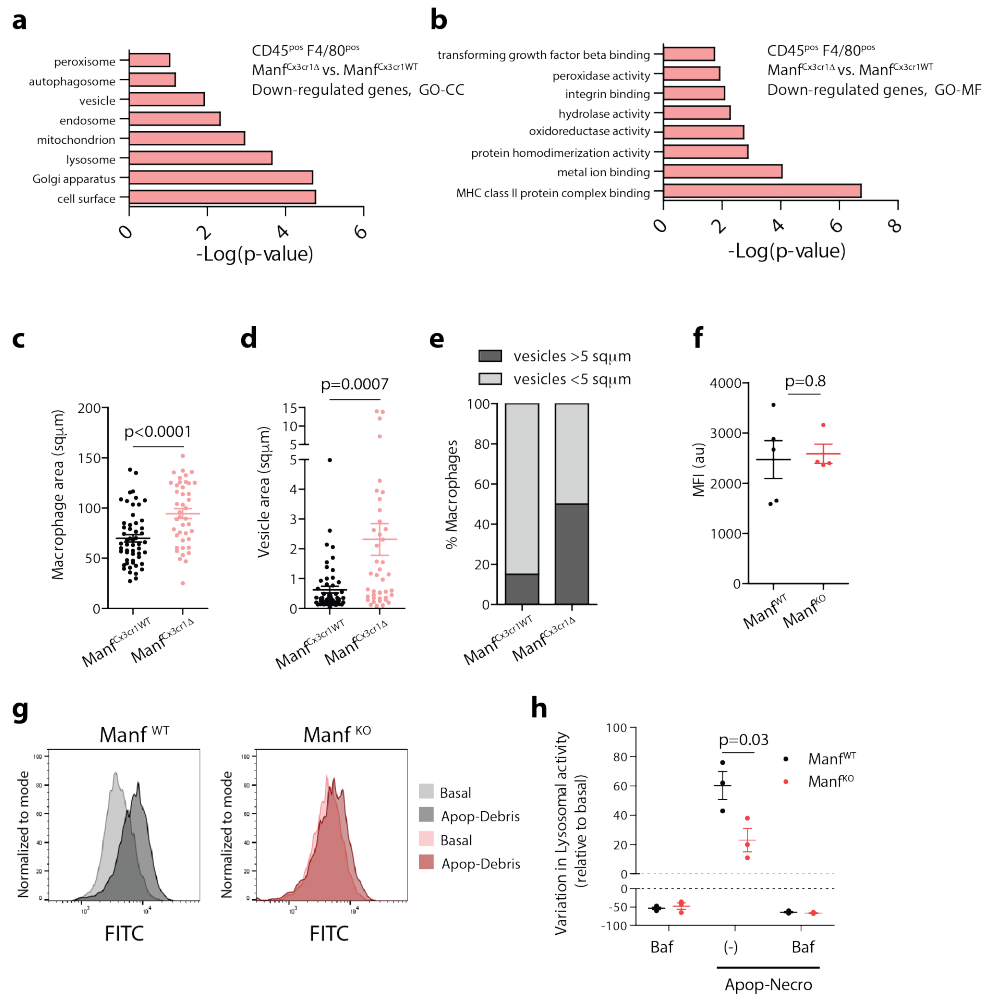
Figure 6

Figure 6. MANF-deficient macrophages have defective lysosomal activity

a,b, GO categories of cellular components (a) and molecular functions (b) showing significant enrichment in the dataset of genes down-regulated in macrophages (CD45^{pos}F4/80^{pos}) FACS-isolated at 3dpi from QC muscles of Manf$^{Cx3cr1\Delta}$ mice compared to Manf^{Cx3cr1WT} mice (fold change<0.75 and p≤0.05, p values from two-tailed Student's t-test, n=3/condition). **c-e,** Quantification of macrophage area (c), intracellular vesicle area (d), and percentage of pro-repair macrophages with at least one vesicle bigger than 5 sqµm (e), in a population of pro-repair macrophages FACS-isolated at 3dpi from quadriceps (QC) muscles of Manf^{Cx3cr1WT} and Manf$^{Cx3cr1\Delta}$ mice (n=54 macrophages, Manf^{Cx3cr1WT} and n= 42 macrophages, Manf$^{Cx3cr1\Delta}$). **f,** MFI of Fluoresbrite 641 signal, quantified by flow cytometry, in Manf^{WT} and Manf^{KO} BMDMs, 3h after stimulation with opsonized Fluoresbrite® 641 Carboxylate beads (n=5 for Manf^{WT}; n=4 for Manf^{KO}). Representative histogram of the Fluoresbrite® 641 signal is shown in Extended data 7b. **g,** Representative histograms of the FITC signal derived from lysosomal hydrolysis of a self-quenched substrate in basal conditions (light) and after stimulation with Apop-necro debris (dark), in BMDMs generated from Manf$^{fl/fl}$ (grey) and Manf$^{R26\Delta}$ (pink) mice, 3h after stimulation. **h,** Lysosomal activity, evaluated by flow cytometry, as the MFI in the FITC channel, in Manf^{WT} and Manf^{KO} BMDMs (n=3/condition), 3h after stimulation with a self-quenched lysosomal substrate and cell debris containing apoptotic and necrotic cells (Apop-Necro). Lysosomal activity is referred to the basal lysosomal activity in each individual BMDM culture. Data are represented as average ± s.e.m. and each n represents one animal or one cell culture derived from one independent animal. p values are from two-tailed Student's t-test. dpi, days post-injury; GO, Gene Ontology; CC, cellular component; MF, molecular function; MFI, Mean Fluorescence intensity; Baf, Bafilomycin.
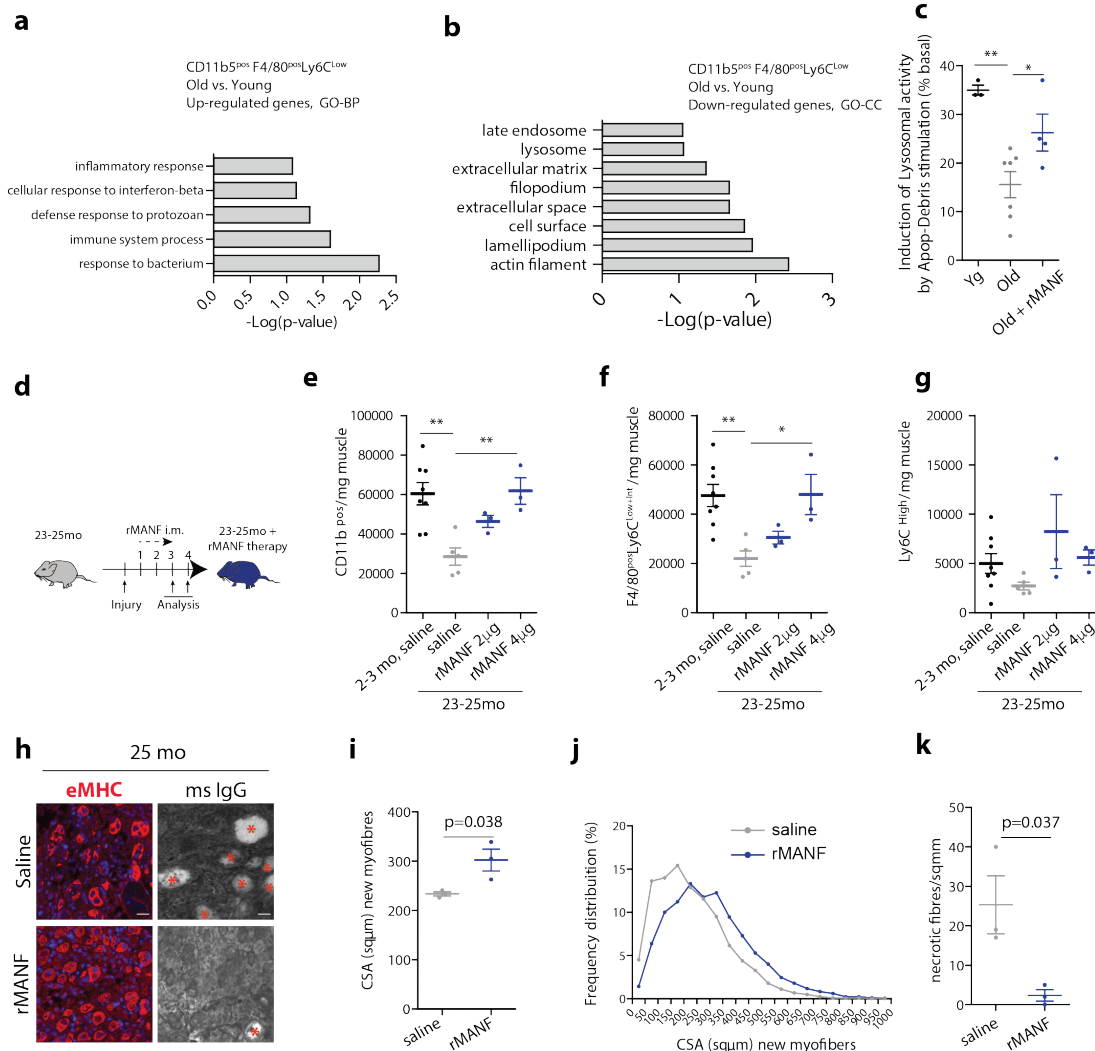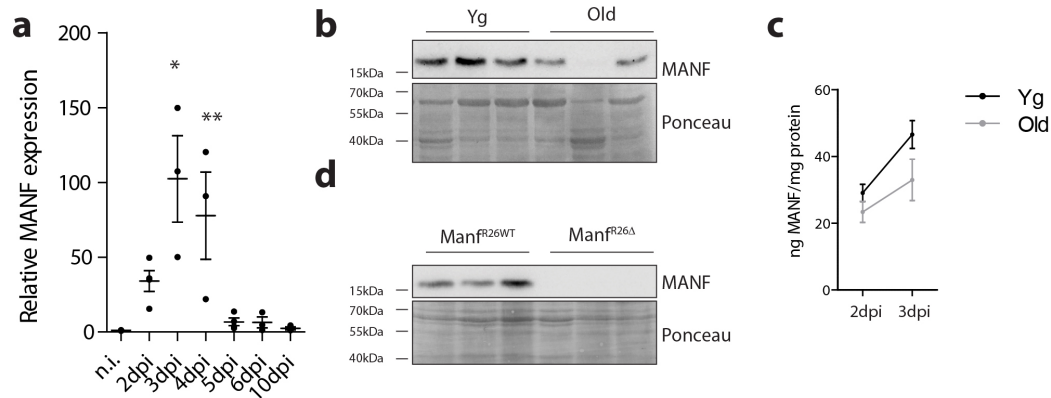
Figure 7

a

CD11b5^{pos} F4/80^{pos}Ly6C^{Low}
Old vs. Young
Up-regulated genes, GO-BP

inflammatory response
cellular response to interferon-beta
defense response to protozoan
immune system process
response to bacterium

-Log(p-value)

b

CD11b5^{pos} F4/80^{pos}Ly6C^{Low}
Old vs. Young
Down-regulated genes, GO-CC

late endosome
lysosome
extracellular matrix
filopodium
extracellular space
cell surface
lamellipodium
actin filament

-Log(p-value)

c

Induction of Lysosomal activity by Apop-Debris stimulation (% basal)

Yg   Old   Old + rMANF

d

23-25mo
rMANF i.m.
23-25mo + rMANF therapy
Injury   Analysis

e

CD11b ^{pos}/mg muscle

2-3 mo, saline   saline   rMANF 2μg   rMANF 4μg
23-25mo

f

F4/80^{pos}Ly6C$^{Low+Int}$/mg muscle

2-3 mo, saline   saline   rMANF 2μg   rMANF 4μg
23-25mo

g

Ly6C ^{High}/mg muscle

2-3 mo, saline   saline   rMANF 2μg   rMANF 4μg
23-25mo

h

25 mo

eMHC   ms IgG

Saline

rMANF

i

CSA (sqμm) new myofibres

p=0.038

saline   rMANF

j

Frequency distribuition (%)

saline
rMANF

CSA (sqμm) new myofibers

k

necrotic fibres/sqmm

p=0.037

saline   rMANF

Figure 7. MANF therapy restores regenerative success in aged skeletal muscles

a,b, GO categories of biological processes (a) and cellular components (b) showing significant enrichment in the dataset of genes up-regulated (a) or down-regulated (b) in pro-repair macrophages (F4/80^{pos}Ly6C^{Low}) FACS-isolated at 3dpi from QC muscles of old (22-24mo) mice compared to yg (2-6mo) mice (fold change<0.75 or >1.5 and p≤0.05, p values from two-tailed Student's t-test, n=3/condition). **c,** Lysossomal activity, evaluated by flow cytometry, as the MFI in the FITC channel, in BMDMs from yg and old mice, with and without rMANF stimulation (n=3 for yg; n=7 for Old; n=4 for Old+rMANF), 3h after stimulation with a self-quenched lysosomal substrate and cell debris containing apoptotic and necrotic cells (Apop-Necro). Lysosomal activity is referred to the basal lysosomal activity in each individual BMDM culture. See also Extended data Fig. 9b. **d,** Experimental timeline for analysis of aged animals with rMANF therapy. **e-g,** Quantification, by flow cytometry, of myeloid cells (CD11b^{pos}, e), pro-repair macrophages (F4/80^{pos}Ly6C$^{Low+Int}$, f) and pro-inflammatory macrophages (Ly6C^{High}, g) in regenerating TA muscles of yg (2-3mo) and old (23-25mo) wt (C57BL/6) mice at 3dpi, treated with i.m. injections of saline or rMANF (n=8 for yg; n=5 for old saline; n=3 for other conditions). **h,** Representative

images of eMHC (red, left) or mouse IgG (right) staining in cryosections of regenerating TA muscles from old (25mo) mice, at 4dpi, treated with intramuscular injections of rMANF or saline. DAPI (blue) is used to identify nuclei. Asterisks indicate necrotic myofibres. **i-k,** Quantification of the average cross-sectional area of new myofibers (i), frequency distribution of new myofibres by size (j) and average number of necrotic fibres (k) in regenerating TA muscles as shown in (h) (n=3/condition). Data are represented as average ± s.e.m. and each n represents one animal. In c, e-g, p values are from one-way ANOVA with Dunnett's multiple comparison post-test. In I and k, p values are from two-tailed Student's t-test. GO, Gene Ontology; BP, biological process; CC, cellular component; i.m., intramuscular injection; rMANF; recombinant Mesencephalic astrocyte-derived neurotrophic factor; eMHC; embryonic myosin heavy chain; ms IgG, mouse Immunoglobulin; CSA, cross-sectional area.

Extended data Figure 1. Regulation of muscle regeneration by MANF

a, Relative levels of MANF mRNA, detected by RT-qPCR, in TA muscles of yg wt (C57BL/6) mice non-injured and at different time points following injury (2, 3, 4, 5, 6, 10 dpi) (n=3 for 3,4,6,10dpi; n=4 for n.i.,2,5dpi). **b,** Illustrative Western blot analysis of MANF levels in protein extracts of TA muscles from yg (2-6mo) and old (22-25mo) wt (C57BL/6) mice at 3dpi. Ponceau S-staining of the membrane was used to verify equal protein loading in each sample. **c,** MANF protein levels, quantified by ELISA, in extracts of TA muscles from yg (2-6mo) and old (22-25mo) wt (C57BL/6) mice, at 2 and 3dpi (n=5 for yg 3dpi; n=3 for all other conditions). **d,** Western blot analysis of MANF levels in protein extracts from Manf^{R26WT} and Manf$^{R26\Delta}$ mice at 3dpi. Ponceau S-staining of the membrane was used to verify equal protein loading in each sample. In a, p values are from one-way ANOVA with Bonferroni's multiple comparison post-test. n.i., non-injured; dpi, days post-injury; yg, young.
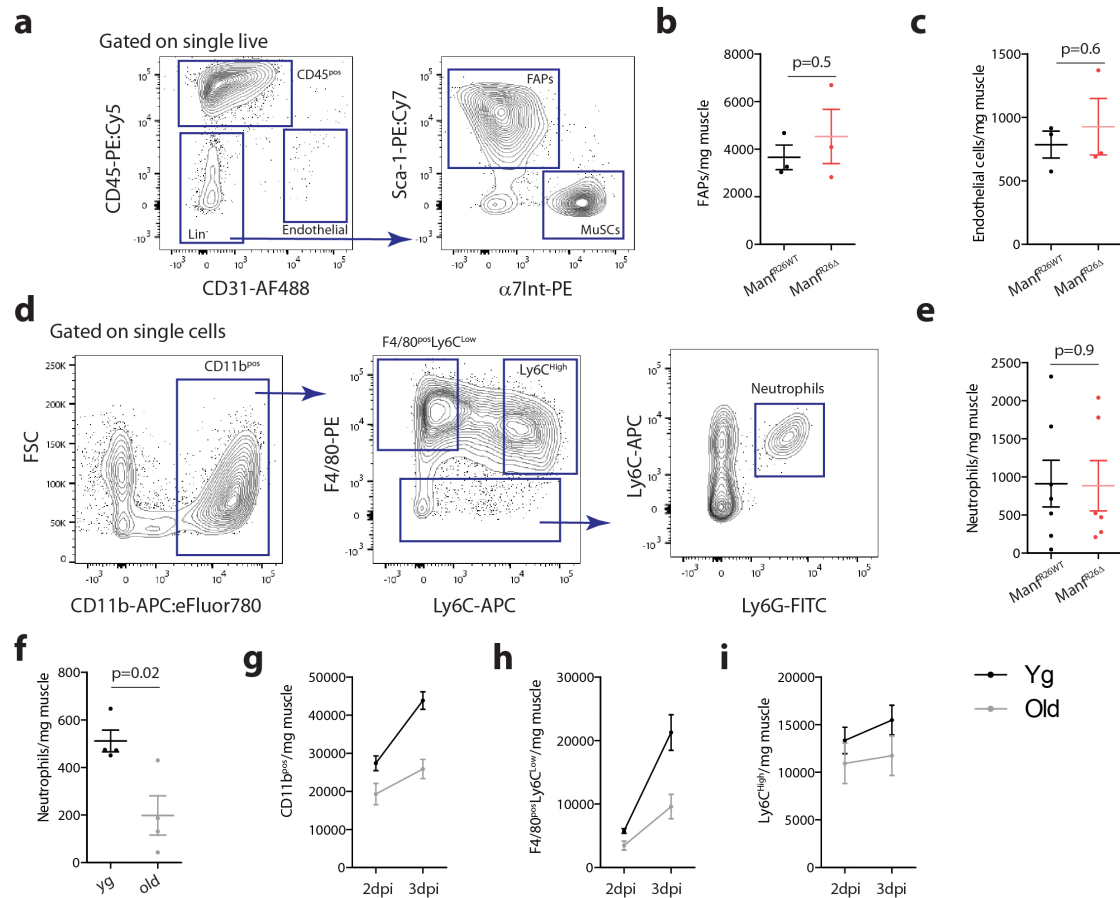
Extended data Figure 2. Effects of aging and MANF-deficiency in the cellular response during muscle regeneration

a,d, Gating strategy used in flow cytometry analysis of (a) CD45^{pos} immune cell population, endothelial cells, FAPs and MuSCs; and (d) myeloid cells (CD11b^{pos}), pro-repair macrophages (F4/80^{pos}Ly6C^{Low}), pro-inflammatory macrophages (LyC6^{High}), and neutrophils (F4/80^{neg}Ly6G^{pos}). **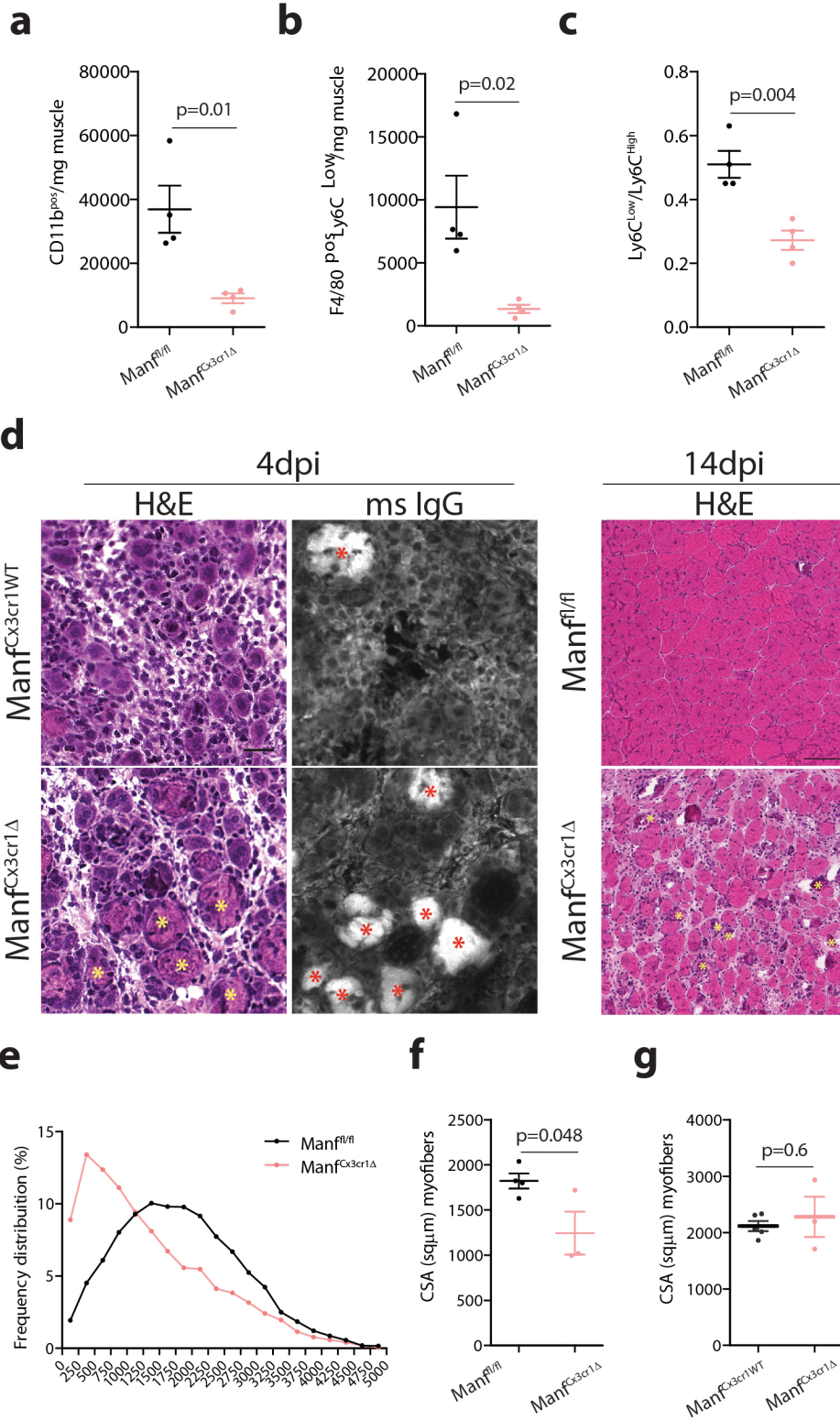b,c,e,f,** Quantification, by flow cytometry, of FAPS (b, n=3/condition), endothelial cells (c, n=3/condition) and neutrophils (e, n=7 for Manf^{R26WT}; n=6 for Manf$^{R26\Delta}$) in regenerating muscles of Manf^{R26WT} and Manf$^{R26\Delta}$ mice at 3dpi; and neutrophils (f, n=4/condition) in regenerating muscles of yg (2-6mo) and old (22-24mo) wt (C57BL/6) mice at 3dpi. **g-i,** Quantification, by flow cytometry, of myeloid cells (CD11b^{pos}, g), pro-repair macrophages (F4/80^{pos}Ly6C^{Low}, h) and pro-inflammatory macrophages (Ly6C^{High}, i) in regenerating muscles of yg (2-6mo) and old (22-25mo) wt (C57BL/6) mice at 2 and 3dpi (n=4 for yg and old 3dpi; n=5 for old 2dpi; n=6 for yg 2dpi). Data are represented as average ± s.e.m. and each n represents one animal. p values are from two-tailed Student's t-test. FAPs, Fibroadipogenic progenitors; MuSCs; Muscle Stem Cells; yg, young.
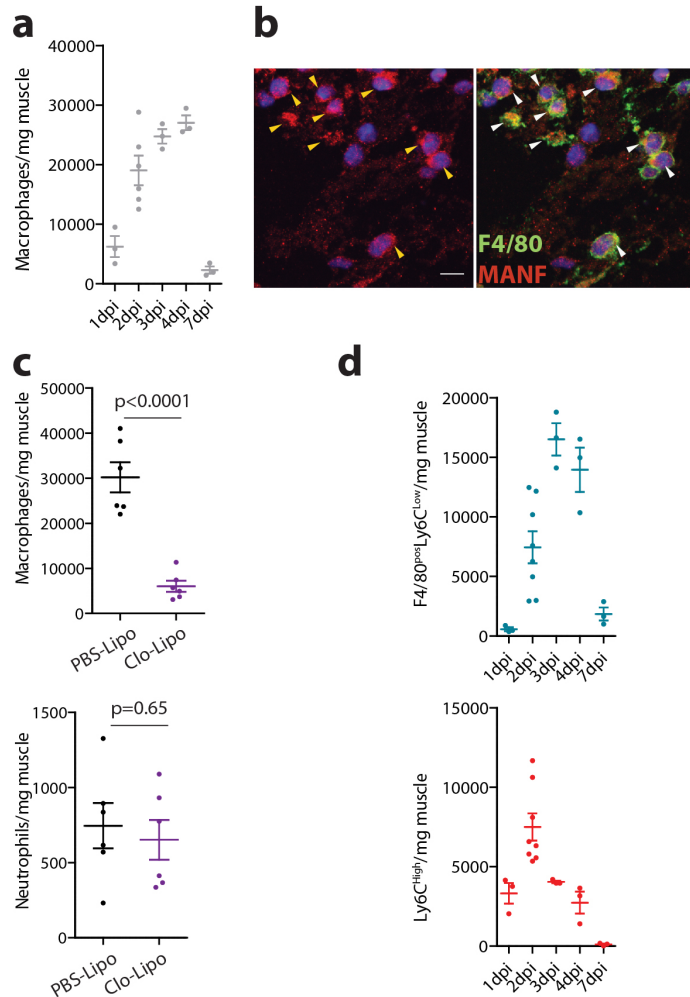
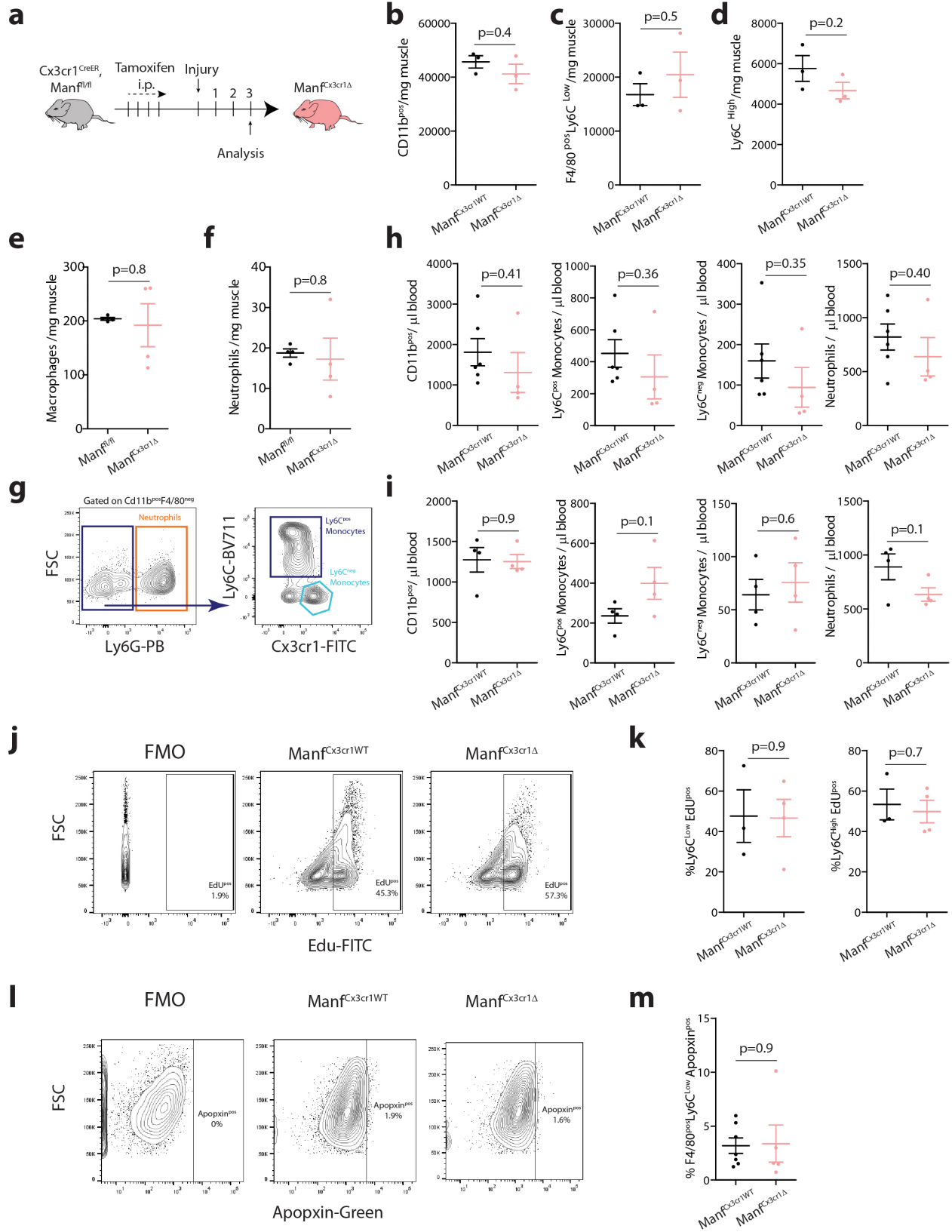**Extended data Figure 3. Macrophage-derived MANF in muscle regeneration**
a,d Quantification, by flow cytometry, of macrophages (a), pro-repair macrophages (d, top; F4/80^{pos}Ly6C^{Low}) and pro-inflammatory macrophages (d, bottom; Ly6C^{High}) in regenerating muscles of wt (C57BL/6) mice at different time points following injury (n=6 for macrophages 2dpi; n=8 for F4/80^{pos}Ly6C^{Low} and Ly6C^{High} at 2dpi; n=3 for all other conditions). **b,** Representative images of cryosections from Tibialis anterior (TA) muscles immunostained against F4/80 (green) and MANF (red). DAPI is used to identify nuclei. Arrowheads indicate cells with high MANF expression co-localized with F4/80. Scale bar: 10µm **c,** Quantification, by flow cytometry, of macrophages and neutrophils in regenerating quadriceps (QC) muscles of wt (C57BL6/J) mice at 3dpi, treated with clodronate liposomes or control PBS liposomes (n=6/condition). Data are represented as average ± s.e.m. and each n represents one animal. p values are from two-tailed Student's t-test. dpi, days post-injury; PBS-Lipo, PBS Liposomes; Clo-Lipo, Clodronate Liposomes.

Extended data Figure 4. Macrophage-derived MANF in muscle regeneration
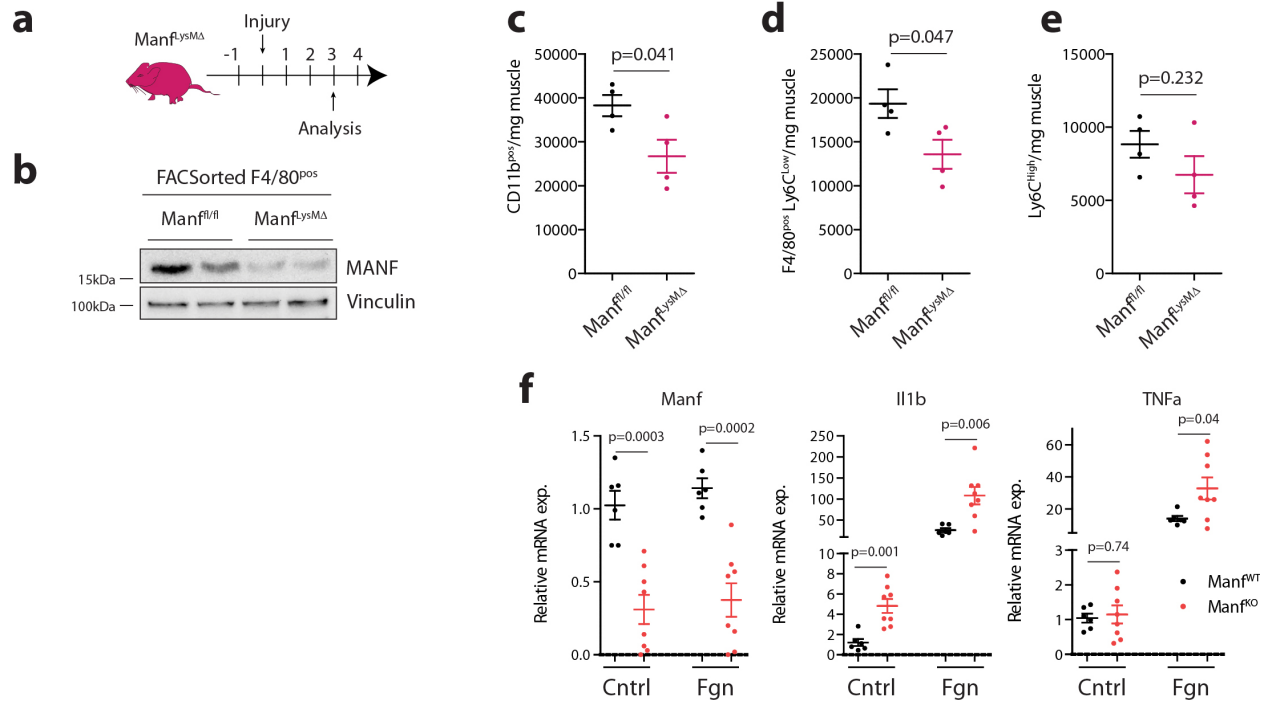**a-c,** Quantification, by flow cytometry, of myeloid cells (CD11b^{pos}, a), pro-repair macrophages (F4/80^{pos}Ly6C^{Low}, b), and ratio of pro-repair to pro-inflammatory macrophages (LyC6^{Low}/LyC6^{High},

c) in regenerating quadriceps (QC) muscles of tamoxifen treated Manf$^{fl/fl}$ and Manf$^{Cx3cr1\Delta}$ mice at 3dpi (n=4/condition). **d,** Representative images of cryosections from Tibialis anterior (TA) muscles of Manf$^{fl/fl}$, Manf^{Cx3cr1WT} and Manf$^{Cx3cr1\Delta}$ mice, at 4 and 14dpi, stained with H&E and immunostained with mouse IgG. Asterisks indicate necrotic myofibres. Scale bars: 50μm for H&E 4dpi; 20μm for IgG 4dpi; 100μm for H&E 14dpi. **e-f,** Quantification of the average cross-sectional area of central nucleated new myofibres (f) and frequency distribution of new myofibres by size (e), in regenerating TA muscles from Manf$^{fl/fl}$ and Manf$^{Cx3cr1\Delta}$ mice at 14dpi (n=4 for Manf$^{fl/fl}$; n=3 for Manf$^{Cx3cr1\Delta}$). **g,** Quantification of the average cross-sectional area of myofibers in non-injured TA muscles from Manf^{Cx3cr1WT} and Manf$^{Cx3cr1\Delta}$ mice (n=5 for Manf^{Cx3cr1WT}; n=3 for Manf$^{Cx3cr1\Delta}$). Data are represented as average ± s.e.m. and each n represents one animal. p values are from two-tailed Student's t-test. dpi, days post-injury; H&E, Hematoxylin and Eosin; msIgG, mouse Immunoglobulin; CSA, cross-sectional area.
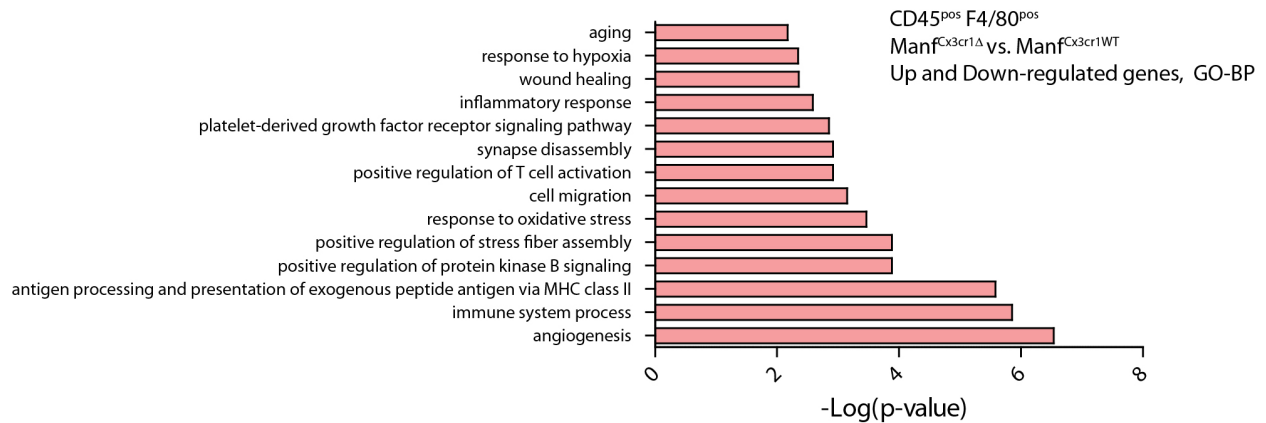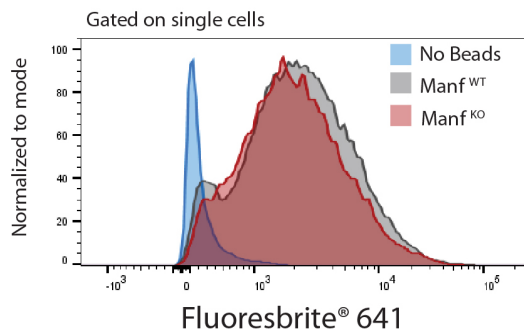
Extended data Figure 5. Effects of MANF ablation in Cx3cr1^{pos} cells

a, Experimental timeline for analysis of animals with conditional ablation of MANF only in Cx3cr1-expressing cells existing prior to muscle injury. **b-d,** Quantification, by flow cytometry, of myeloid cells (CD11b^{pos}, b), pro-repair macrophages (F4/80^{pos}Ly6C^{Low}, c), and pro-inflammatory macrophages (LyC6^{High}, d) in 3dpi regenerating QC muscles of Manf^{Cx3cr1WT} and Manf$^{Cx3cr1\Delta}$ mice, treated with tamoxifen prior to the injury (n=3/condition). **e-f,** Quantification, by flow cytometry, of macrophages (CD11b^{pos}F4/80^{pos}, e) and neutrophils (CD11b^{pos}F4/80^{neg}Ly6G^{pos}, f) non-injured QC muscles of tamoxifen treated Manf$^{fl/fl}$ and Manf$^{Cx3cr1\Delta}$ mice (n=4/condition). **g,** Representative density plots from flow cytometry analysis of myeloid blood cell populations gated on CD11b^{pos}F4/80^{neg} population, identifying neutrophils (Ly6G^{pos}), Ly6C^{pos} classical monocytes (Ly6G^{neg}Ly6C^{pos}) and Ly6C^{neg} non-classical monocytes (Ly6G^{neg}Ly6C^{neg}Cx3cr1^{pos}). **h-i,** Quantification, by flow cytometry, of myeloid cells (CD11b^{pos}), Ly6C^{pos} classical monocytes, Ly6C^{neg} non-classical monocytes and neutrophils in the blood of Manf^{Cx3cr1WT} and Manf$^{Cx3cr1\Delta}$ mice prior to muscle injury (h, n=6 for Manf^{Cx3cr1WT}; n=4 for Manf$^{Cx3cr1\Delta}$), and at 3dpi (i, n=4/ condition). **j,l,** Representative density plots from flow cytometry analysis of macrophage populations from Manf^{Cx3cr1WT} and Manf$^{Cx3cr1\Delta}$ animals at 3dpi, showing EdU signal (j) and Apopxin-Green signal (l). For both stains the FMO density plot is shown to define the positive population. **k,** Quantification, by flow cytometry, of EdU^{pos} macrophages as a percentage of pro-repair and pro-inflammatory populations, in Manf^{Cx3cr1WT} and Manf$^{Cx3cr1\Delta}$ animals at 3dpi (n=3 for Manf^{Cx3cr1WT}; n=4 for Manf$^{Cx3cr1\Delta}$). **m,** Quantification, by flow cytometry, of Apopxin^{pos} macrophages as a percentage of pro-repair the population, in Manf^{Cx3cr1WT} and Manf$^{Cx3cr1\Delta}$ animals at 3dpi (n=7 for Manf^{Cx3cr1WT}; n=5 for Manf$^{Cx3cr1\Delta}$). Data are represented as average ± s.e.m. and each n represents one animal. p values are from two-tailed Student's t-test. FSC, Forward Scatter; Edu, 5-ethynyl-2'-deoxyuridine; FMO, Fluorescence Minus One Control.

Extended data Figure 6. MANF-deficiency affects macrophage phenotypic transition and inflammatory status

a, Experimental timeline for analysis of animals with ablation of MANF in macrophages. **b,** Western blot analysis of MANF levels in protein extracts from F4/80^{pos} cells FACS-isolated from QC muscles of Manf$^{fl/fl}$ and Manf$^{LysM\Delta}$ mice at 3dpi. Vinculin was used to verify equal protein loading in each sample. **c-e,** Quantification, by flow cytometry, of myeloid cells (CD11b^{pos}, c), pro-repair macrophages (F4/80^{pos}Ly6C^{Low}, d) and pro-inflammatory macrophages (LyC6^{High}, e) in regenerating QC muscles of Manf$^{fl/fl}$ and Manf$^{LysM\Delta}$ mice at 3dpi (n=4/condition). **f,** Relative levels of Manf, Il1β and TNFα mRNA, detected by RT-qPCR, in BMDMs generated from Manf$^{fl/fl}$ and Manf$^{R26\Delta}$ mice in control conditions or 3h after stimulation with Fibrinogen (n= 6 for Manf^{WT} and n=8 for Manf^{KO}). Data are represented as average ± s.e.m. and each n represents one animal or one cell culture derived from one independent animal. p values are from two-tailed Student's t-test. BMDMs, Bone marrow-derived macrophages; Fgn, Fibrinogen.

a

CD45^{pos} F4/80^{pos}
Manf$^{Cx3cr1\Delta}$ vs. Manf^{Cx3cr1WT}
Up and Down-regulated genes, GO-BP

Bar chart categories (top to bottom):
aging
response to hypoxia
wound healing
inflammatory response
platelet-derived growth factor receptor signaling pathway
synapse disassembly
positive regulation of T cell activation
cell migration
response to oxidative stress
positive regulation of stress fiber assembly
positive regulation of protein kinase B signaling
antigen processing and presentation of exogenous peptide antigen via MHC class II
immune system process
angiogenesis

x-axis: -Log(p-value)

b

Gated on single cells

Legend:
No Beads
Manf^{WT}
Manf^{KO}

y-axis: Normalized to mode
x-axis: Fluoresbrite® 641

Extended Data Figure 7. Defects of MANF-deficient macrophages

a, GO categories of biological processes showing significant enrichment in the dataset of genes differentially expressed in macrophages (CD45^{pos}F4/80^{pos}) FACS-isolated at 3dpi from quadriceps muscles of Manf$^{Cx3cr1\Delta}$ mice compared to Manf^{Cx3cr1WT} mice (fold change<0.75 or >1.5 and p≤0.05, p values from two-tailed Student's t-test, n=3/condition). **b,** Representative histogram of the Fluoresbrite® 641 signal in BMDMs generated from Manf$^{fl/fl}$ (grey) and Manf$^{R26\Delta}$ (pink) mice, 3h after stimulation with opsonized Fluoresbrite® 641 Carboxylate beads. Signal in non-stimulated BMDMs is shown in blue. BMDMs, Bone marrow-derived macrophages.

Manf^{Cx3cr1WT}

2 um

Manf$^{Cx3cr1\Delta}$

2 um
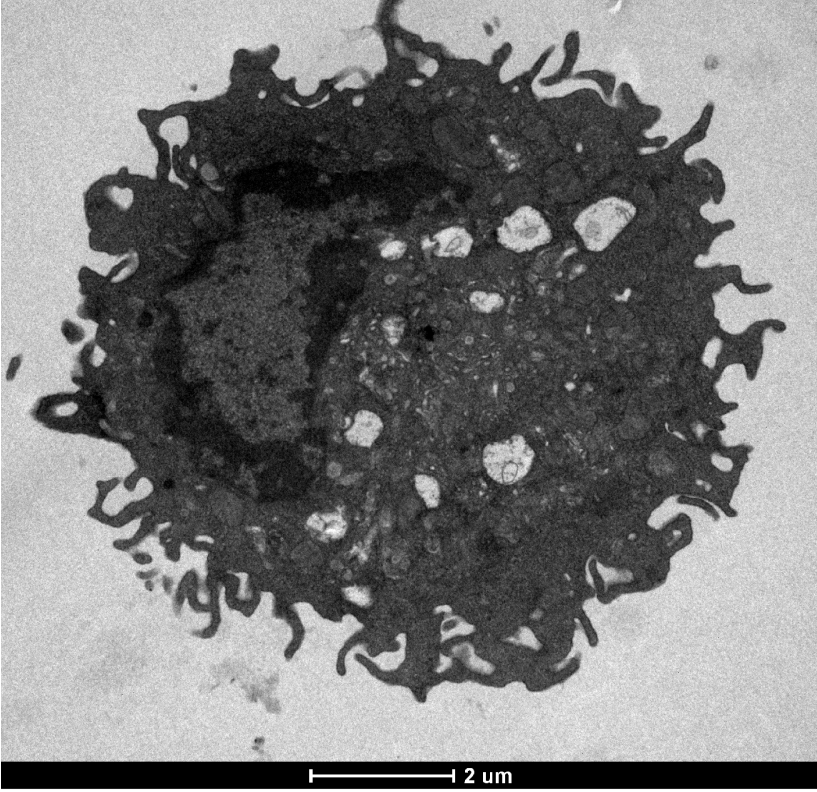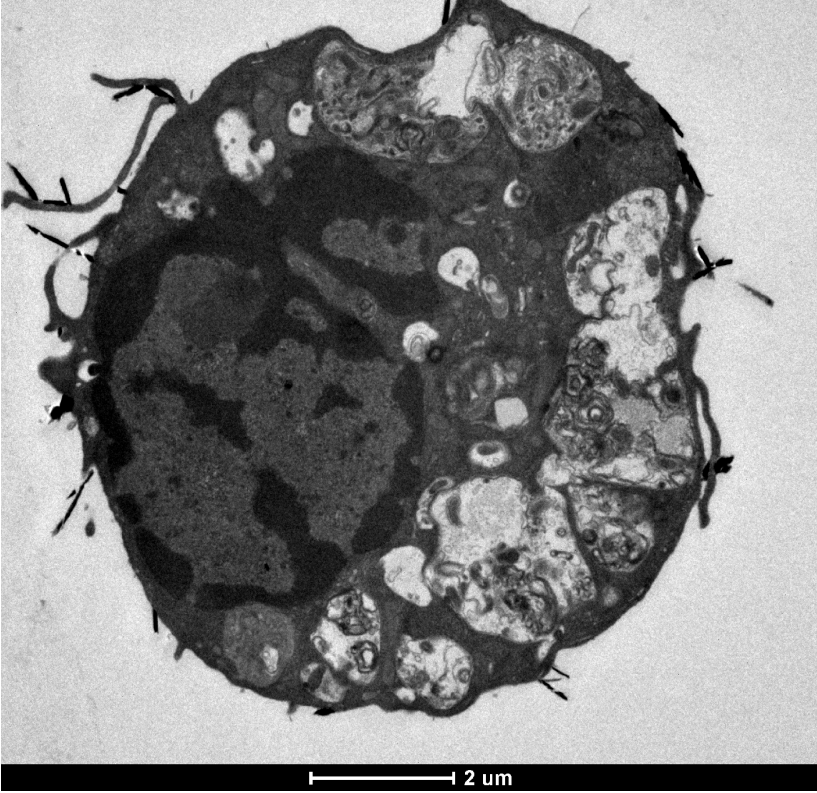
Extended Data Figure 8. Transmission electron microscopy analysis MANF-deficient and macrophages

Representative images of pro-repair macrophages (F4/80^{pos}Ly6C^{Low}) FACS-isolated at 3dpi from QC muscles of Manf^{Cx3cr1WT} and Manf$^{Cx3cr1\Delta}$ mice, analyzed by TEM. Scale bars: 2µm Quantifications of these images, for independent cells, are shown in Fig. 6c-e. The quantification includes 54 macrophages isolated from Manf^{Cx3cr1WT} mice and 42 macrophages isolated from Manf$^{Cx3cr1\Delta}$ mice. Macrophages were sorted from n=3 animals/condition in 2 independent experiments (experiment 1: n=1/condition; experiment 2: n=2/condition, pooled). Samples obtained in each experiment were processed independently for analysis.

a

CD11b^{pos} F4/80^{pos}Ly6C^{Low}
Old vs. Young
Down-regulated genes, GO-BP
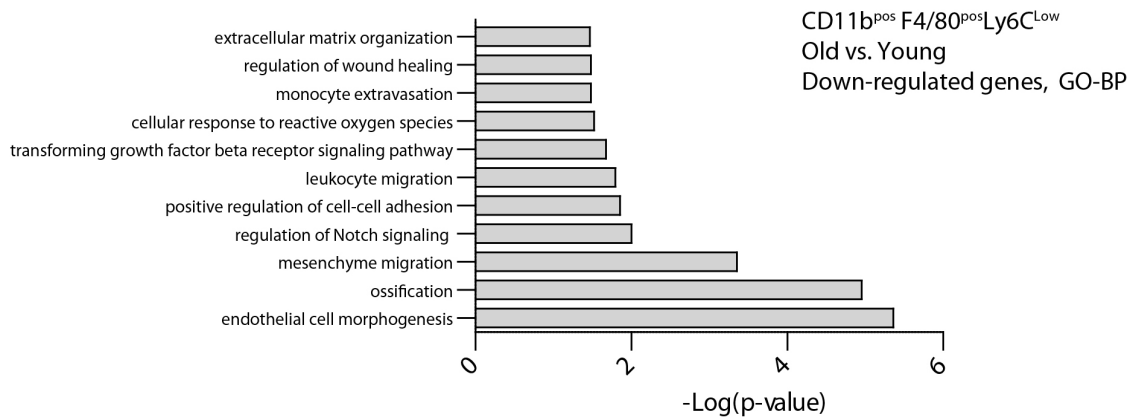
b
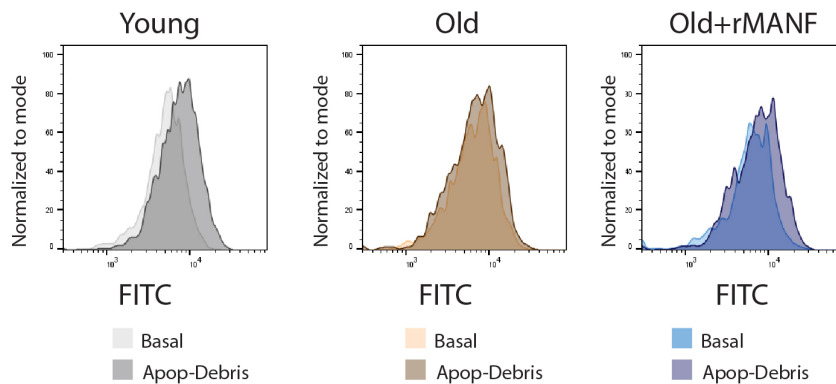
Extended Data Figure 9. Defects of aged macrophages

a, GO categories of biological processes with relevance within the context of tissue regeneration showing significant enrichment in the dataset of genes down-regulated in pro-repair macrophages (CD11b^{pos}F4/80^{pos}Ly6C^{Low}) FACS-isolated at 3dpi from quadriceps muscles of old (22-24mo) mice compared to yg (2-6mo) mice (fold change <0.75 and p≤0.05, p values from two-tailed Student's t-test, n=3/condition). **e,** Representative histograms of the FITC signal derived from lysosomal hydrolysis of a self-quenched substrate in basal conditions (light) and after stimulation with Apop-necro debris (dark), in BMDMs generated from yg (grey) and old (brown) mice, and in old BMDMs cultured in the presence of rMANF (blue), 3h after stimulation. GO, Gene Ontology; BP, Biological process; BMDMs, Bone marrow-derived macrophages.

Supplementary Table 1
Primer list for genotyping.

Allele	Size (bp)	Forward Primer	Reverse Primer
MANF Wt	512	TGAAGCAAGAGGCAAAGAGAATCGG	TGCTCAGCTGCAGAGTTAGAGTTCC
MANF fl	718	TGAAGCAAGAGGCAAAGAGAATCGG	TGCTCAGCTGCAGAGTTAGAGTTCC
Cx3Cr1 wt	695	AAGACTCACGTGGACCTGCT	CGGTTATTCAACTTGCACCA
Cx3Cr1 Cre-ER	300	AGGATGTTGACTTCCGAGTTG	CGGTTATTCAACTTGCACCA
R26 wt	198	CTG GCT TCT GAG GAC CG	CCG AAA ATC TGT GGG AAG TC
R26 Cre-ER	150	CGT GAT CTG CAA CTC CAG TC	AGG CAA ATT TTG TGT ACG G
LyzM WT	350	TTA CAG TCG GCC AGG CTG AC	CTT GGG CTG CCA GAA TTT CTC
LyzM Cre	700	CCC AGA AAT GCC AGA TTA CG	

Supplementary Table 2
Primary Antibodies for IHC

Target Gene	Species	Source	Dilution
MANF	rabbit	Sigma (SAB3500384)	1:300
F4/80	rat	BioRad (MCA497G)	1:40
eMHC	mouse	D.S.H.B (F1.652)	Non-diluted

Supplementary Table 3
Fluorophore-conjugated antibodies for FC analysis and FACS

Fluorophore	Antibody	Source	Dilution
FITC	Anti-mouse CD45	Biolegend (103107)	1:200
PE	Anti-mouse F4/80	Biolegend (123110)	1:50
APC	Anti-mouse Ly6C	eBioscience™ (17-5932-82)	1:200
FITC	Anti-mouse Ly6G	Biolegend (127606)	1:400
APC-eFluor®780	Anti-mouse CD11b	eBioscience™ (47-0112-82)	1:200
Alexa Fluor488	Anti-mouse CD31	Biolegend (102513)	1:50
PE-Cy5	Anti-mouse CD45	Biolegend (103109)	1:100
PE-Cy7	Anti-mouse Sca-1	Biolegend (108113)	1:100
PE	Anti-mouse α7integrin	Miltenyi Biotec (130-120-812)	1:40
Pacific Blue™	Anti-mouse Ly6G	Biolegend (127612)	1:50
FITC	Anti-mouse CX3CR1	Biolegend (149019)	1:800
Brilliant Violet 711™	Anti-mouse Ly6C	Biolegend (128037)	1:40
APC	Anti-mouse F4/80	Biolegend (123116)	1:100
FITC	Anti-mouse Ly6C	Biolegend (128006)	1:200

Supplementary Table 4
Primary antibodies for WB

Target Gene	Species	Source	Dilution in WB
MANF	rabbit	Sigma (SAB3500384)	1:1000
Beta-Actin	mouse	DSHB (JLA-20C)	1:200
Vinculin	mouse	Sigma (V9131)	1:2000

Supplementary Table 5
Primer list for RT-qPCR

Gene	Species	Forward Primer	Reverse Primer
MANF	mouse	GCTGCCACCAAGATCATCAA	CACAGGGATATGGTGGGCC
Beta-actin	mouse	GCTCTGGCTCCTAGCACCAT	GCCACCGATCCACACAGAGT
Cx3cr1	mouse	CTTTATCTACGCCTTTGCC	CTTCCTATACAGGTGTCCC
Tnfα	mouse	TTCTCATTCCTGCTTGTGG	TTGGGAACTTCTCATCCCT
IL1β	mouse	CCTCAATGGACAGAATATCAACC	GATCCACACTCTCCAGCTG

References

1   Neves, J., Sousa-Victor, P. & Jasper, H. Rejuvenating Strategies for Stem Cell-Based Therapies in Aging. *Cell stem cell* **20**, 161-175, doi:10.1016/j.stem.2017.01.008 (2017).
2   Schultz, M. B. & Sinclair, D. A. When stem cells grow old: phenotypes and mechanisms of stem cell aging. *Development* **143**, 3-14, doi:10.1242/dev.130633 (2016).
3   Conboy, I. M. *et al.* Rejuvenation of aged progenitor cells by exposure to a young systemic environment. *Nature* **433**, 760-764, doi:10.1038/nature03260 (2005).
4   Conboy, I. M., Conboy, M. J. & Rebo, J. Systemic Problems: A perspective on stem cell aging and rejuvenation. *Aging* **7**, 754-765, doi:10.18632/aging.100819 (2015).
5   Ruckh, J. M. *et al.* Rejuvenation of regeneration in the aging central nervous system. *Cell stem cell* **10**, 96-103, doi:10.1016/j.stem.2011.11.019 (2012).
6   Neves, J. & Sousa-Victor, P. Regulation of inflammation as an anti-aging intervention. *The FEBS journal* **287**, 43-52, doi:10.1111/febs.15061 (2020).
7   Yousefzadeh, M. J. *et al.* An aged immune system drives senescence and ageing of solid organs. *Nature* **594**, 100-105, doi:10.1038/s41586-021-03547-7 (2021).
8   Wosczyna, M. N. & Rando, T. A. A Muscle Stem Cell Support Group: Coordinated Cellular Responses in Muscle Regeneration. *Developmental cell* **46**, 135-143, doi:10.1016/j.devcel.2018.06.018 (2018).
9   Sousa-Victor, P., Garcia-Prat, L. & Munoz-Canoves, P. Control of satellite cell function in muscle regeneration and its disruption in ageing. *Nature reviews. Molecular cell biology* **23**, 204-226, doi:10.1038/s41580-021-00421-2 (2022).
10   Munoz-Canoves, P., Neves, J. & Sousa-Victor, P. Understanding muscle regenerative decline with aging: new approaches to bring back youthfulness to aged stem cells. *The FEBS journal* **287**, 406-416, doi:10.1111/febs.15182 (2020).
11   Tidball, J. G. Regulation of muscle growth and regeneration by the immune system. *Nature reviews. Immunology* **17**, 165-178, doi:10.1038/nri.2016.150 (2017).
12   Chazaud, B. Inflammation and Skeletal Muscle Regeneration: Leave It to the Macrophages! *Trends in immunology* **41**, 481-492, doi:10.1016/j.it.2020.04.006 (2020).
13   Arnold, L. *et al.* Inflammatory monocytes recruited after skeletal muscle injury switch into antiinflammatory macrophages to support myogenesis. *The Journal of experimental medicine* **204**, 1057-1069, doi:10.1084/jem.20070075 (2007).
14   Perdiguero, E. *et al.* p38/MKP-1-regulated AKT coordinates macrophage transitions and resolution of inflammation during tissue repair. *The Journal of cell biology* **195**, 307-322, doi:10.1083/jcb.201104053 (2011).

15   Neves, J. *et al.* Immune modulation by MANF promotes tissue repair and regenerative success in the retina. *Science* **353**, aaf3646, doi:10.1126/science.aaf3646 (2016).

16   Jntti, M. & Harvey, B. K. Trophic activities of endoplasmic reticulum proteins CDNF and MANF. *Cell and tissue research* **382**, 83-100, doi:10.1007/s00441-020-03263-0 (2020).

17   Sousa-Victor, P., Jasper, H. & Neves, J. Trophic Factors in Inflammation and Regeneration: The Role of MANF and CDNF. *Frontiers in physiology* **9**, 1629, doi:10.3389/fphys.2018.01629 (2018).

18   Lindahl, M., Saarma, M. & Lindholm, P. Unconventional neurotrophic factors CDNF and MANF: Structure, physiological functions and therapeutic potential. *Neurobiology of disease* **97**, 90-102, doi:10.1016/j.nbd.2016.07.009 (2017).

19   Tang, Q., Li, Y. & He, J. MANF: an emerging therapeutic target for metabolic diseases. *Trends in endocrinology and metabolism: TEM* **33**, 236-246, doi:10.1016/j.tem.2022.01.001 (2022).

20   Sousa-Victor, P. *et al.* MANF regulates metabolic and immune homeostasis in ageing and protects against liver damage. *Nature metabolism* **1**, 276-290, doi:10.1038/s42255-018-0023-6 (2019).

21   Neves, J. *et al.* MANF delivery improves retinal homeostasis and cell replacement therapies in ageing mice. *Experimental gerontology* **134**, 110893, doi:10.1016/j.exger.2020.110893 (2020).

22   Sousa-Victor, P. *et al.* Geriatric muscle stem cells switch reversible quiescence into senescence. *Nature* **506**, 316-321, doi:10.1038/nature13013 (2014).

23   Rahman, F. A., Angus, S. A., Stokes, K., Karpowicz, P. & Krause, M. P. Impaired ECM Remodeling and Macrophage Activity Define Necrosis and Regeneration Following Damage in Aged Skeletal Muscle. *International journal of molecular sciences* **21**, doi:10.3390/ijms21134575 (2020).

24   Mircescu, M. M., Lipuma, L., van Rooijen, N., Pamer, E. G. & Hohl, T. M. Essential role for neutrophils but not alveolar macrophages at early time points following Aspergillus fumigatus infection. *The Journal of infectious diseases* **200**, 647-656, doi:10.1086/600380 (2009).

25   Kowalski, E. A. *et al.* Monocyte proinflammatory phenotypic control by ephrin type A receptor 4 mediates neural tissue damage. *JCI insight* **7**, doi:10.1172/jci.insight.156319 (2022).

26   Lehmann, M. L. *et al.* CCR2 monocytes repair cerebrovascular damage caused by chronic social defeat stress. *Brain, behavior, and immunity* **101**, 346-358, doi:10.1016/j.bbi.2022.01.011 (2022).

27   Varga, T. *et al.* Highly Dynamic Transcriptional Signature of Distinct Macrophage Subsets during Sterile Inflammation, Resolution, and Tissue Repair. *J Immunol* **196**, 4771-4782, doi:10.4049/jimmunol.1502490 (2016).

28   Wang, Y., Welc, S. S., Wehling-Henricks, M. & Tidball, J. G. Myeloid cell-derived tumor necrosis factor-alpha promotes sarcopenia and regulates muscle cell fusion with aging muscle fibers. *Aging cell* **17**, e12828, doi:10.1111/acel.12828 (2018).

29   Wang, Y. *et al.* Aging of the immune system causes reductions in muscle stem cell populations, promotes their shift to a fibrogenic phenotype, and modulates sarcopenia. *FASEB journal : official publication of the Federation of American Societies for Experimental Biology* **33**, 1415-1427, doi:10.1096/fj.201800973R (2019).

30   Runyan, C. E. *et al.* Impaired phagocytic function in CX3CR1(+) tissue-resident skeletal muscle macrophages prevents muscle recovery after influenza A virus-induced pneumonia in old mice. *Aging cell* **19**, e13180, doi:10.1111/acel.13180 (2020).

31   Tobin, S. W. *et al.* Delineating the relationship between immune system aging and myogenesis in muscle repair. *Aging cell* **20**, e13312, doi:10.1111/acel.13312 (2021).

32   Patsalos, A. *et al.* In vivo GDF3 administration abrogates aging related muscle regeneration delay following acute sterile injury. *Aging cell* **17**, e12815, doi:10.1111/acel.12815 (2018).

33   Summan, M. *et al.* Macrophages and skeletal muscle regeneration: a clodronate-containing liposome depletion study. *American journal of physiology. Regulatory, integrative and comparative physiology* **290**, R1488-1495, doi:10.1152/ajpregu.00465.2005 (2006).

34   Sahu, A. *et al.* Age-related declines in alpha-Klotho drive progenitor cell mitochondrial dysfunction and impaired muscle regeneration. *Nature communications* **9**, 4859, doi:10.1038/s41467-018-07253-3 (2018).

35   Wehling-Henricks, M. *et al.* Macrophages escape Klotho gene silencing in the mdx mouse model of Duchenne muscular dystrophy and promote muscle growth and increase satellite cell numbers through a Klotho-mediated pathway. *Human molecular genetics* **27**, 14-29, doi:10.1093/hmg/ddx380 (2018).

36   Zhang, C. *et al.* Age-related decline of interferon-gamma responses in macrophage impairs satellite cell proliferation and regeneration. *Journal of cachexia, sarcopenia and muscle* **11**, 1291-1305, doi:10.1002/jcsm.12584 (2020).

37   Paliwal, P., Pishesha, N., Wijaya, D. & Conboy, I. M. Age dependent increase in the levels of osteopontin inhibits skeletal muscle regeneration. *Aging* **4**, 553-566, doi:10.18632/aging.100477 (2012).

38   Tidball, J. G., Flores, I., Welc, S. S., Wehling-Henricks, M. & Ochi, E. Aging of the immune system and impaired muscle regeneration: A failure of immunomodulation of adult myogenesis. *Experimental gerontology* **145**, 111200, doi:10.1016/j.exger.2020.111200 (2021).

39   Al-Zaeed, N., Budai, Z., Szondy, Z. & Sarang, Z. TAM kinase signaling is indispensable for proper skeletal muscle regeneration in mice. *Cell death & disease* **12**, 611, doi:10.1038/s41419-021-03892-5 (2021).

40   Petrova, P. *et al.* MANF: a new mesencephalic, astrocyte-derived neurotrophic factor with selectivity for dopaminergic neurons. *Journal of molecular neuroscience : MN* **20**, 173-188, doi:10.1385/jmn:20:2:173 (2003).

41   Voutilainen, M. H. *et al.* Mesencephalic astrocyte-derived neurotrophic factor is neurorestorative in rat model of Parkinson's disease. *The Journal of neuroscience : the official journal of the Society for Neuroscience* **29**, 9651-9659, doi:10.1523/JNEUROSCI.0833-09.2009 (2009).

42   Lu, J. *et al.* Photoreceptor Protection by Mesencephalic Astrocyte-Derived Neurotrophic Factor (MANF). *eNeuro* **5**, doi:10.1523/ENEURO.0109-18.2018 (2018).

43   Glembotski, C. C. *et al.* Mesencephalic astrocyte-derived neurotrophic factor protects the heart from ischemic damage and is selectively secreted upon sarco/endoplasmic reticulum calcium depletion. *The Journal of biological chemistry* **287**, 25893-25904, doi:10.1074/jbc.M112.356345 (2012).

44   Zhang, Y. *et al.* Hormonal therapies up-regulate MANF and overcome female susceptibility to immune checkpoint inhibitor myocarditis. *Science translational medicine* **14**, eabo1981, doi:10.1126/scitranslmed.abo1981 (2022).

45   He, M. *et al.* Mesencephalic astrocyte-derived neurotrophic factor ameliorates steatosis in HepG2 cells by regulating hepatic lipid metabolism. *World journal of gastroenterology* **26**, 1029-1041, doi:10.3748/wjg.v26.i10.1029 (2020).

46   Lindahl, M. *et al.* MANF is indispensable for the proliferation and survival of pancreatic beta cells. *Cell reports* **7**, 366-375, doi:10.1016/j.celrep.2014.03.023 (2014).

47   Herranen, A. *et al.* Deficiency of the ER-stress-regulator MANF triggers progressive outer hair cell death and hearing loss. *Cell death & disease* **11**, 100, doi:10.1038/s41419-020-2286-6 (2020).

48   Han, D. *et al.* Mesencephalic astrocyte-derived neurotrophic factor restores blood-brain barrier integrity of aged mice after ischaemic stroke/reperfusion through anti-inflammation via

TLR4/MyD88/NF-kappaB pathway. *Journal of drug targeting* **30**, 430-441, doi:10.1080/1061186X.2021.2003803 (2022).

49   Yang, F. *et al.* Bone marrow mesenchymal stem cells induce M2 microglia polarization through PDGF-AA/MANF signaling. *World journal of stem cells* **12**, 633-658, doi:10.4252/wjsc.v12.i7.633 (2020).

50   Zhang, J. X. *et al.* Mesencephalic astrocyte-derived neurotrophic factor (MANF) prevents the neuroinflammation induced dopaminergic neurodegeneration. *Experimental gerontology* **171**, 112037, doi:10.1016/j.exger.2022.112037 (2023).

51   Tonkin, J. *et al.* Monocyte/Macrophage-derived IGF-1 Orchestrates Murine Skeletal Muscle Regeneration and Modulates Autocrine Polarization. *Molecular therapy : the journal of the American Society of Gene Therapy* **23**, 1189-1200, doi:10.1038/mt.2015.66 (2015).

52   Zhao, W., Lu, H., Wang, X., Ransohoff, R. M. & Zhou, L. CX3CR1 deficiency delays acute skeletal muscle injury repair by impairing macrophage functions. *FASEB journal : official publication of the Federation of American Societies for Experimental Biology* **30**, 380-393, doi:10.1096/fj.14-270090 (2016).

53   Pakarinen, E. *et al.* MANF Ablation Causes Prolonged Activation of the UPR without Neurodegeneration in the Mouse Midbrain Dopamine System. *eNeuro* **7**, doi:10.1523/ENEURO.0477-19.2019 (2020).

54   Pakarinen, E., Lindholm, P., Saarma, M. & Lindahl, M. CDNF and MANF regulate ER stress in a tissue-specific manner. *Cellular and molecular life sciences : CMLS* **79**, 124, doi:10.1007/s00018-022-04157-w (2022).

55   Roy, A. *et al.* The IRE1/XBP1 signaling axis promotes skeletal muscle regeneration through a cell non-autonomous mechanism. *eLife* **10**, doi:10.7554/eLife.73215 (2021).

56   Chen, L. *et al.* Mesencephalic astrocyte-derived neurotrophic factor is involved in inflammation by negatively regulating the NF-kappaB pathway. *Scientific reports* **5**, 8133, doi:10.1038/srep08133 (2015).

57   Oh, J. *et al.* Age-associated NF-kappaB signaling in myofibers alters the satellite cell niche and re-strains muscle stem cell function. *Aging* **8**, 2871-2896, doi:10.18632/aging.101098 (2016).

58   Yagi, T. *et al.* Neuroplastin Modulates Anti-inflammatory Effects of MANF. *iScience* **23**, 101810, doi:10.1016/j.isci.2020.101810 (2020).

59   Ren, H., Xia, X., Dai, X. & Dai, Y. The role of neuroplastin65 in macrophage against E. coli infection in mice. *Molecular immunology* **150**, 78-89, doi:10.1016/j.molimm.2022.08.003 (2022).

60   Sereno, D. *et al.* An evolutionary perspective on the role of mesencephalic astrocyte-derived neurotrophic factor (MANF): At the crossroads of poriferan innate immune and apoptotic pathways. *Biochemistry and biophysics reports* **11**, 161-173, doi:10.1016/j.bbrep.2017.02.009 (2017).

61   Doyle, S. E. *et al.* Toll-like receptors induce a phagocytic gene program through p38. *The Journal of experimental medicine* **199**, 81-90, doi:10.1084/jem.20031237 (2004).

62   Ortuste Quiroga, H. P., Goto, K. & Zammit, P. S. Isolation, Cryosection and Immunostaining of Skeletal Muscle. *Methods Mol Biol* **1460**, 85-100, doi:10.1007/978-1-4939-3810-0_8 (2016).

63   Bencze, M., Periou, B., Baba-Amer, Y. & Authier, F. J. Immunolabelling Myofiber Degeneration in Muscle Biopsies. *Journal of visualized experiments : JoVE*, doi:10.3791/59754 (2019).

64   Galli, E. *et al.* Mesencephalic Astrocyte-Derived Neurotrophic Factor Is Upregulated with Therapeutic Fasting in Humans and Diet Fat Withdrawal in Obese Mice. *Scientific reports* **9**, 14318, doi:10.1038/s41598-019-50841-6 (2019).